Numerical Simulation of Oxygen and Hydrocarbon Coupled Biodegradation and Diffusion in the Vadose Zone

by L. Richard Peterson

1.0 Introduction

When spills or leaks impact soils, or wastes are placed in landfills, the potential for contamination via vapor migration to enclosed spaces (buildings, conduits, etc.) or leachate migration to the groundwater is possible. These two pathways play an important role in decision-making management.

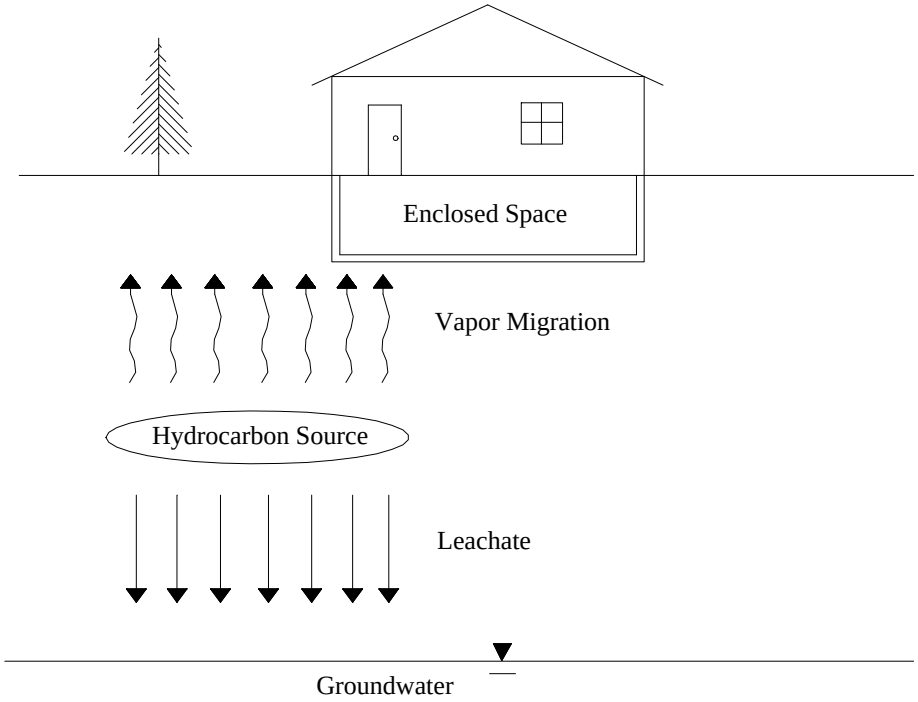

Figure 1-1. General vadose zone contamination schematic.

Current regulations have evolved with leachate impacts on groundwater in mind; however, only recently has the issue of vapor migration been quantitatively and formally considered. This focus has been brought about mainly by the move toward more structured risk-based corrective action (RBCA) approaches.

The risk associated with vapor intrusion and the potential remediation by natural attenuation of vapors in the vadose zone is currently a hot topic (Johnson 1998). Many feel that the current models are too conservative and lead to unnecessary low cleanup levels. The fact that these models generally do not take into account biodegradation may explain these feelings.

It can be hypothesized that some chemicals degrade as they migrate, especially those from petroleum spills (e.g., benzene). If this is true, then these chemicals should be found at concentrations less than those predicted by the current models which neglect natural attenuation. Unfortunately, little data exist to quantify this degree of over-conservatism. This lack of data is a result of many factors, including the fact that interest in this pathway is relatively new.

Vapors in enclosed spaces pose two levels of concern. First, enclosed-space vapors may be found at concentrations near those that pose immediate health risks. These sites warrant immediate attention as required by most state and federal regulatory guidelines. In the second class of sites, concentrations are lower and the concern is for long term health risks. It is these lower concentrations that will be dealt with here.

The mechanisms that impact these pathways (volatilization, biodegradation, leaching, etc.) also control the rate at which vadose zone hydrocarbon sources dissipate over time. Thus in assessing the natural attenuation of vapors and leachates, we can also gain valuable information concerning the longevity of vadose zone hydrocarbon sources.

A common scenario consists of a separate phase source (Zone II) with an unsaturated zone above (Zone I). On occasion there is also an unsaturated zone below (Zone III) as illustrated in Figure 1-2. Under this scenario, we can simulate the shrinking of the separate phase contamination plume.

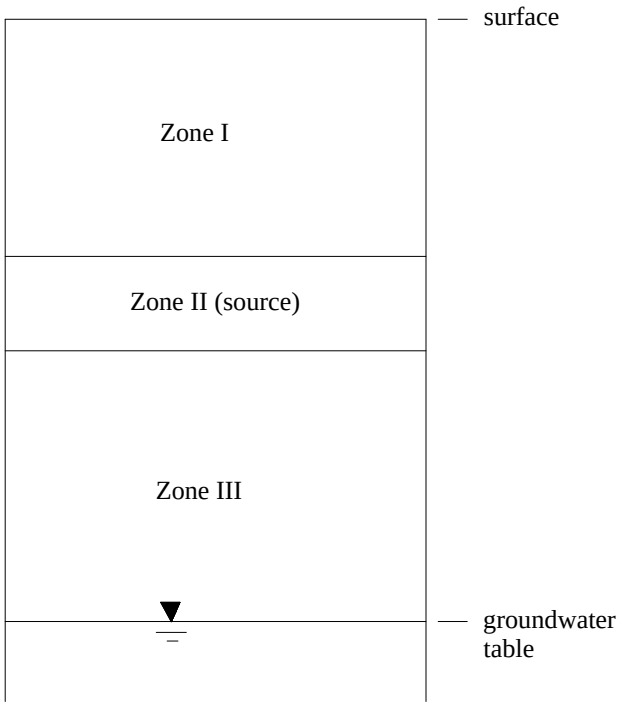

Figure 1-2. A common physical scenario.

2.0 Model Development

In order to assess and predict the fate and migration of hydrocarbon sources in the vadose zone, we begin by developing a simple model. This model will simulate the diffusion of hydrocarbon and oxygen in the vapor and aqueous phases of the unsaturated zone as well as the degradation due to biological factors. The vapor transport of oxygen and hydrocarbon is thus a coupled balance of diffusion and biological degradation. Advection will be neglected by assuming no pressure, thermal, or density gradients exist in the vadose zone. For our purposes we have developed a single component model.

Hydrocarbon Transport

The general governing transport equation for hydrocarbon fate and transport is

$$\frac{\partial M}{\partial t} = \nabla J - \delta \tag{2.1}$$

where:

M – hydrocarbon mass storage per unit volume,
J – flux (vapor and aqueous phases), and
δ – hydrocarbon decay from biodegradation.

The flux gradient in the two phases are described by Fick's 2nd Law:

$$\nabla J = \frac{\partial}{\partial x}\left(D^{e}{}_{w} \frac{\partial C}{\partial x} \right) + \frac{\partial}{\partial x}\left(D^{e}{}_{a} \frac{\partial G}{\partial x} \right) \tag{2.2}$$

where:

C – aqueous hydrocarbon concentration (M/L^3),
G – vapor hydrocarbon concentration (M/L^3),
x – vertical distance (L),
D^{e}_{w} – effective aqueous diffusion coefficient of the hydrocarbon (L^2/T), and
D^{e}_{a} – effective vapor diffusion coefficient of the hydrocarbon (L^2/T).

These coefficients are found by using the classic Millington-Quirk (Millington and Quirk 1961) model

$$D^{e}{}_{w} = \frac{D_w \theta_w^{10/3}}{\phi^2} \tag{2.3}$$

and

$$D^{e}{}_{a} = \frac{D_a \theta_a^{10/3}}{\phi^2} \tag{2.4}$$

where:

D_w – aqueous diffusion coefficient of the hydrocarbon (L^2/T),
D_a – vapor diffusion coefficient of the hydrocarbon (L^2/T),
θ_w – volumetric water content (dimensionless),
θ_a – volumetric air content (dimensionless), and
ϕ – porosity (dimensionless).

If we assume the degradation term follows duel-Monod kinetics first proposed by Rich (1973) and used by others (Borden and Bedient 1985; MacQuarrie 1990; and McClure 1996), we get

$$\delta = \theta_w M_t k_m \left(\frac{C}{K_s + C} \right) \left(\frac{C_{O_2}}{K_{s,O_2} + C_{O_2}} \right) \tag{2.5}$$

where:

M_t – microbial mass concentration (M/L^3),
k_m – maximum substrate utilization rate (T^{-1}),
C_{O_2} – oxygen concentration in the aqueous phase (M/L^3),
K_s – hydrocarbon half-saturation constant (M/L^3), and
K_{s,O_2} – oxygen half-saturation constant (M/L^3).

The total mass per unit volume in the system can be found using values for each of the three phases: soil, water, and air

$$M = \rho_b S + \theta_w C + \theta_a G \tag{2.6}$$

where:

ρ_b – soil bulk density (M/L^3), and

S – hydrocarbon concentration in the soil (M/M).

We can then write the governing equation for hydrocarbon fate and transport as:

$$\frac{\partial}{\partial t}\left(\rho_b S + \theta_w C + \theta_a G\right) = \frac{\partial}{\partial x}\left(D^e{}_w \frac{\partial C}{\partial x}\right) + \frac{\partial}{\partial x}\left(D^e{}_a \frac{\partial G}{\partial x}\right) - \theta_w M_t k_m \left(\frac{C}{K_s + C}\right)\left(\frac{C_{O_2}}{K_{s,O_2} + C_{O_2}}\right) \tag{2.7}$$

We now utilize the concept of total concentration (C_T or O_T), which is the same as equation 2.6 (mass per unit volume).

$$C_T = \rho_b S + \theta_w C + \theta_a G = R_w C = R_a G \tag{2.8}$$

and

$$O_T = \theta_w C_{o_2} + \theta_a G_{O_2} = R_{w,O_2} C_{O_2} = R_{a,O_2} G_{O_2} \tag{2.9}$$

The effective partitioning coefficients are

$$R_w = \rho_b K_d + \theta_w + \theta_a H \tag{2.10}$$

$$R_a = \frac{\rho_b K_d}{H} + \frac{\theta_w}{H} + \theta_a \tag{2.11}$$

$$R_{w,O_2} = \theta_w + \theta_a H_{O_2} \tag{2.12}$$

$$R_{a,O_2} = \frac{\theta_w}{H_{O_2}} + \theta_a \tag{2.13}$$

and

$$K_d = \frac{S}{C} \qquad H = \frac{G}{C} \tag{2.14}$$

$$H_{O_2} = \frac{G_{O_2}}{C_{O_2}} \tag{2.15}$$

where:

R_w – effective water partitioning coefficient for hydrocarbon (dimensionless),
R_a – effective air partitioning coefficient for hydrocarbon (dimensionless),
R_{w,O_2} – effective water partitioning coefficient for oxygen (dimensionless),
R_{a,O_2} – effective air partitioning coefficient for oxygen (dimensionless),
K_d – soil/water partitioning coefficient (L^3/M),
H – air/water partitioning coefficient for the hydrocarbon (Henry's Law constant) (dimensionless),
H_{O_2} – air/water partitioning coefficient for oxygen (Henry's Law constant) (dimensionless), and
G_{O_2} – oxygen concentration in the vapor phase (M/L^3).

Here we obtain the final governing equation for hydrocarbon fate and transport:

$$\frac{\partial C_T}{\partial t} = \frac{\partial}{\partial x}\left(D^e{}_w \frac{\partial (C_T / R_w)}{\partial x} \right) + \frac{\partial}{\partial x}\left(D^e{}_a \frac{\partial (C_T / R_a)}{\partial x} \right) - \theta_w M_t k_m \left(\frac{C_T}{K_s R_w + C_T} \right)\left(\frac{O_T}{K_{s,O_2} R_{w,O_2} + O_T} \right) \tag{2.16}$$

Oxygen Transport

The general governing fate and transport equation for oxygen is similarly defined as:

$$\Delta M^* = \nabla J^* - \delta^* \tag{2.17}$$

where:
M^* – O_2 mass storage,
J^* – O_2 flux (vapor and aqueous phases), and
δ^* – O_2 uptake from biodegradation.

The flux gradient in the two phases are described by similarly

$$\nabla J^* = \frac{\partial}{\partial x}\left(D^e{}_{w,O_2} \frac{\partial C_{O_2}}{\partial x} \right) + \frac{\partial}{\partial x}\left(D^e{}_{a,O_2} \frac{\partial G_{O_2}}{\partial x} \right) \tag{2.18}$$

where:
$D^e{}_{w,O_2}$ – effective aqueous diffusion coefficient of oxygen (L^2/T), and
$D^e{}_{a,O_2}$ – effective vapor diffusion coefficient of oxygen (L^2/T).

These diffusion coefficients are found again by (Millington and Quirk 1961)

$$D^e{}_{w,O_2} = \frac{D_{w,O_2} \theta_w^{10/3}}{\phi^2} \tag{2.19}$$

and

$$D^e{}_{a,O_2} = \frac{D_{a,O_2} \theta_a^{10/3}}{\phi^2} \tag{2.20}$$

where:
D_{w,O_2} – aqueous diffusion coefficient of oxygen (L^2/T), and

D_{a,O_2} – vapor diffusion coefficient of oxygen (L^2/T).

Again we assume the degradation term follows duel-Monod kinetics we get

$$\delta^* = \theta_w M_t k_m F \left(\frac{C_{O_2}}{K_{s,O_2} + C_{O_2}} \right) \left(\frac{C}{K_s + C} \right) \tag{2.21}$$

where:

F – utilization ratio for hydrocarbon to oxygen consumed (dimensionless).

The total mass per unit volume in the system can be found using values for each of the two phases: water and air.

$$\begin{aligned} \frac{\partial}{\partial t}\left(\theta_w C_{O_2} + \theta_a G_{O_2}\right) = \frac{\partial}{\partial x}\left(D^e{}_{w,O_2} \frac{\partial C_{O_2}}{\partial x} \right) + \frac{\partial}{\partial x}\left(D^e{}_{a,O_2} \frac{\partial G_{O_2}}{\partial x} \right) \\ - \theta_w M_t k_m F \left(\frac{C_{O_2}}{K_{s,O_2} + C_{O_2}} \right) \left(\frac{C}{K_s + C} \right) \end{aligned} \tag{2.22}$$

We now see the final oxygen transport equation to be

$$\begin{aligned} \frac{\partial O_T}{\partial t} = \frac{\partial}{\partial x}\left(D^e{}_{a,O_2} \frac{\partial\left(O_T / R_{a,O_2}\right)}{\partial x} \right) + \frac{\partial}{\partial x}\left(D^e{}_{w,O_2} \frac{\partial\left(O_T / R_{w,O_2}\right)}{\partial x} \right) \\ - \theta_w M_t k_m F \left(\frac{O_T}{K_{s,O_2} R_{w,O_2} + O_T} \right) \left(\frac{C_T}{K_s R_w + C_T} \right) \end{aligned} \tag{2.23}$$

The Behavior of Separate Phase

The equation for hydrocarbon in Zone II simulates the shrinking of the source contaminant and essentially the shrinking of the zone itself. The amount of source contaminant that leaves the zone is accounted for one-dimensionally using the following equation:

$$\frac{\partial(\text{Mass})}{\partial t} = \frac{\partial x'}{\partial t} \theta_o \rho_o = \left(D_a^e \frac{\partial(C_T / R_a)}{\partial x} + D_w^e \frac{\partial(C_T / R_w)}{\partial x} \right) \tag{2.24}$$

where:

x’ – vertical shrinking distance diffused (see Figure 2-2) (L),

ρ_o – the specific density of the hydrocarbon (M/L^3), and

θ_o – hydrocarbon content (dimensionless).

Since we are dealing with only one dimension, we assume a depth and width of 1 meter for dimensional consistency.

Typical Boundary Conditions and Initial Conditions

We solve the diffusion part numerically by applying appropriate initial (IC) and boundary (BC) conditions. For oxygen there is only one zone and therefore we need only one governing equation, one IC, and one set of BC’s.

$$@\, t = 0 \qquad C_{O_2} = C_i \ \ mg/L \ \ (aq) \tag{2.25}$$

$$@\, x = 0 \ \ (\text{surface}) \qquad C_{O_2} = C_i \ \ mg/L \ \ (aq) \tag{2.26}$$

$$@\, x = L_3 \ \ (\text{gw table}) \qquad \frac{\partial O_T}{\partial t} = 0 \tag{2.27}$$

where:

C_i – oxygen concentration in the aqueous phase (M/L^3),

We assume C_i to be the equilibrium concentration of oxygen due to normal temperature and atmospheric conditions and calculated using the ideal gas law. The no flow condition described by equation 2.27 allows oxygen vapor concentrations to reach C_i levels when we neglect biodegradation.

For hydrocarbon we need one equation, one IC and one set of BC's for each zone. If we use the typical scenario as shown in Figure 1-2, we get the following conditions for Zone I

$$@\, t = 0 \qquad C_T = 0 \tag{2.28}$$

$$@\, x = 0 \ \ (\text{surface}) \qquad C_T = 0 \tag{2.29}$$

$$@\, x = L_1 \qquad C = C_O \tag{2.30}$$

where:

C_o – hydrocarbon equilibrium concentration in the aqueous phase (M/L^3).

The explanation for the zero concentration at the surface for the hydrocarbon is due to the fact that at the surface there is a much higher wind circulation affect just above the soil or basement foundation compared to just below in the soil subsurface. Hence the vapor will be "swept" away once they reach this boundary. The initial conditions are based upon the assumption that we have a clean vadose zone before vapors begin to diffuse away from the separate phase source.

For the source zone (Zone II), we need only the IC of separate phase liquid with an equilibrium concentration specified (C_o).

For Zone III we get:

$$@\, t = 0 \qquad C_T = 0 \tag{2.31}$$

$$@\, x = L_2 \qquad C = C_O \tag{2.32}$$

$$@\, x = L_3 \ \ (\text{gw table}) \qquad \frac{\partial C_T}{\partial t} = 0 \tag{2.33}$$

Similar to Zone I for the hydrocarbon, we get the IC and the BC at bottom of the source. The BC at the water table describes a "no flow" condition where the relative flow of vapors cease at the water table. There would still be some partitioning into the water phase but the aqueous phase diffusion is a much slower process and hence the BC is valid.

Integrated Finite Difference Approach

We solve these equations by splitting up the partial differential governing equation 2.16 into two parts: the process describing diffusion and the process describing biodegradation

diffusion

$$\left(\frac{\partial C_T}{\partial t}\right)_D = \frac{\partial}{\partial x}\left(D^e{}_w \frac{\partial (C_T / R_w)}{\partial x}\right) + \frac{\partial}{\partial x}\left(D^e{}_a \frac{\partial (C_T / R_a)}{\partial x}\right) \tag{2.34}$$

biodegradation

$$\left(\frac{\partial C_T}{\partial t}\right)_B = -\theta_w M_t k_m \left(\frac{C_T}{K_s R_w + C_T}\right)\left(\frac{O_T}{K_{s,O_2} R_{w,O_2} + O_T}\right) \tag{2.35}$$

The diffusion part for hydrocarbon (2.34) is solved numerically as in

$$\begin{aligned}
\Delta x_i \frac{C_i^{n+1} - C_i^n}{\Delta t} = {} & \omega\left[\frac{(D^e{}_a)_{i+1/2}}{\Delta x_{i+1/2}}\left(\frac{C_{i+1}^{n+1}}{Ra_{i+1}} - \frac{C_i^{n+1}}{Ra_i}\right) + \frac{(D^e{}_a)_{i-1/2}}{\Delta x_{i-1/2}}\left(\frac{C_{i-1}^{n+1}}{Ra_{i-1}} - \frac{C_i^{n+1}}{Ra_i}\right)\right] + \\
& \omega\left[\frac{(D^e{}_w)_{i+1/2}}{\Delta x_{i+1/2}}\left(\frac{C_{i+1}^{n+1}}{Rw_{i+1}} - \frac{C_i^{n+1}}{Rw_i}\right) + \frac{(D^e{}_w)_{i-1/2}}{\Delta x_{i-1/2}}\left(\frac{C_{i-1}^{n+1}}{Rw_{i-1}} - \frac{C_i^{n+1}}{Rw_i}\right)\right] + \\
& (1-\omega)\left[\frac{(D^e{}_a)_{i+1/2}}{\Delta x_{i+1/2}}\left(\frac{C_{i+1}^{n}}{Ra_{i+1}} - \frac{C_i^{n}}{Ra_i}\right) + \frac{(D^e{}_a)_{i-1/2}}{\Delta x_{i-1/2}}\left(\frac{C_{i-1}^{n}}{Ra_{i-1}} - \frac{C_i^{n}}{Ra_i}\right)\right] + \\
& (1-\omega)\left[\frac{(D^e{}_w)_{i+1/2}}{\Delta x_{i+1/2}}\left(\frac{C_{i+1}^{n}}{Rw_{i+1}} - \frac{C_i^{n}}{Rw_i}\right) + \frac{(D^e{}_w)_{i-1/2}}{\Delta x_{i-1/2}}\left(\frac{C_{i-1}^{n}}{Rw_{i-1}} - \frac{C_i^{n}}{Rw_i}\right)\right]
\end{aligned} \tag{2.36}$$

where:

ω – weighting factor.

$$\Delta x_i = \frac{1}{2}\left(\Delta x_{i+1/2} + \Delta x_{i-1/2}\right) \tag{2.37}$$

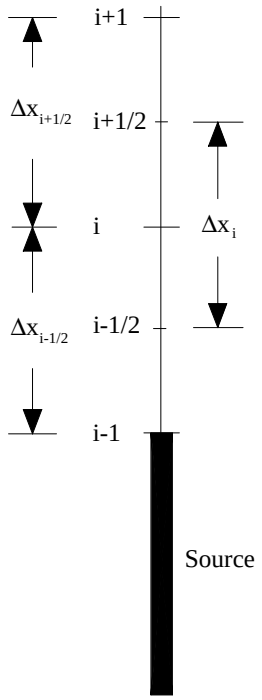

Figure 2-1. Schematic of cell numbering scheme.

Using the Gauss-Seidel iterative method, we solve equation 2.36 with an error bound of 0.001 (Yakowitz and Szidarovszky 1989). The partial differential governing equation for oxygen (2.23) is solved and split up in a similar manner.

diffusion

$$\left(\frac{\partial O_T}{\partial t}\right)_D = \frac{\partial}{\partial x}\left(D^e{}_{a,O_2}\frac{\partial\left(O_T/R_{a,O_2}\right)}{\partial x}\right)+\frac{\partial}{\partial x}\left(D^e{}_{w,O_2}\frac{\partial\left(O_T/R_{w,O_2}\right)}{\partial x}\right) \tag{2.38}$$

biodegradation

$$\left(\frac{\partial O_T}{\partial t}\right)_B = -\theta_w M_t\left(\frac{O_T}{K_{s,O_2}R_{w,O_2}+O_T}\right)F\,k_m\left(\frac{C_T}{K_s R_w + C_T}\right) \tag{2.39}$$

The parts describing biodegradation (2.35) and (2.39) are solved using the 4th order Runge-Kutta algorithm as in

$$\left(\frac{\partial C_T}{\partial t}\right)_B = -\theta_w M_t k_m\left(\frac{C_T}{K_s R_w + C_T}\right)\left(\frac{O_T}{K_{s,O_2}R_{w,O_2}+O_T}\right)= F^1 \tag{2.40}$$

$$\left(\frac{\partial O_T}{\partial t}\right)_B = -\theta_w M_t\left(\frac{O_T}{K_{s,O_2}R_{w,O_2}+O_T}\right)F\,k_m\left(\frac{C_T}{K_s R_w + C_T}\right)= F^2 \tag{2.41}$$

$$F_1^1 = F^1\left(O_T, C_T\right) \tag{2.42}$$

$$F_1^2 = F^2\left(O_T, C_T\right) \tag{2.43}$$

$$F_2^1 = F^1\left(O_T + \frac{1}{2}h\,F_1^2, C_T + \frac{1}{2}h\,F_1^1\right) \tag{2.44}$$

$$F_2^2 = F^2\left(O_T + \frac{1}{2}h\,F_1^2, C_T + \frac{1}{2}h\,F_1^1\right) \tag{2.45}$$

$$F_3^1 = F^1\left(O_T + \frac{1}{2}h\,F_2^2, C_T + \frac{1}{2}h\,F_2^1\right) \tag{2.46}$$

$$F_3^2 = F^2\left(O_T + \frac{1}{2}h\,F_2^2, C_T + \frac{1}{2}h\,F_2^1\right) \tag{2.47}$$

$$F_4^1 = F^1\left(O_T + \frac{1}{2}h\,F_3^2, C_T + \frac{1}{2}h\,F_3^1\right) \tag{2.48}$$

$$F_4^2 = F^2\left(O_T + \frac{1}{2}h\,F_3^2, C_T + \frac{1}{2}h\,F_3^1\right) \tag{2.49}$$

Then we find that the concentrations at the next time step are found by

$$F^1(t+\Delta h) = F^1(t) + \frac{h}{6}\left(F_1^1 + 2\cdot F_2^1 + 2\cdot F_3^1 + F_4^1\right) \tag{2.50}$$

and

$$F^2(t+\Delta h) = F^2(t) + \frac{h}{6}\left(F_1^2 + 2\cdot F_2^2 + 2\cdot F_3^2 + F_4^2\right) \tag{2.51}$$

It is believed that time scales for the transport and biodegradation processes are different. The biodegradation time step (Δh) should be smaller than the transport time step (Δt), since the diffusion process is much slower than the reaction process. This approach is called time splitting. However upon closer analysis we find no significant difference in concentration results between 1:1 and 1:10 ratios. The 1:5 ratio is the most common and is used by Kemblowski and Ma (1994) where Δt is 5 times larger than Δh. With increased speed and memory storage capacity of computers, we may see the concept of time splitting disappear in the future. Since we have chosen small time steps, there is no need for time splitting in our simulation.

We then take a first order approximation of equation 2.24 to get

$$\text{Mass} = \Delta x'\theta_o\rho_o = \Delta t\left(D^e{}_a\frac{\partial(C_T/R_a)}{\partial x} + D^e{}_w\frac{\partial(C_T/R_w)}{\partial x}\right) \tag{2.52}$$

where:

ρ_o – specific density of the hydrocarbon.

$$\Delta x' = \frac{\Delta t \omega}{\theta_o \rho_o}\left[\frac{(D^e{}_a)_{i-1/2}}{\Delta x_{i-1/2}}\left(\frac{C_{i-1}^{n+1}}{Ra_{i-1}} - \frac{C_i^{n+1}}{Ra_i}\right) + \frac{(D^e{}_w)_{i-1/2}}{\Delta x_{i-1/2}}\left(\frac{C_{i-1}^{n+1}}{Rw_{i-1}} - \frac{C_i^{n+1}}{Rw_i}\right)\right] + \frac{\Delta t(1-\omega)}{\theta_o \rho_o}\left[\frac{(D^e{}_a)_{i-1/2}}{\Delta x_{i-1/2}}\left(\frac{C_{i-1}^{n}}{Ra_{i-1}} - \frac{C_i^{n}}{Ra_i}\right) + \frac{(D^e{}_w)_{i-1/2}}{\Delta x_{i-1/2}}\left(\frac{C_{i-1}^{n}}{Rw_{i-1}} - \frac{C_i^{n}}{Rw_i}\right)\right] \quad (2.53)$$

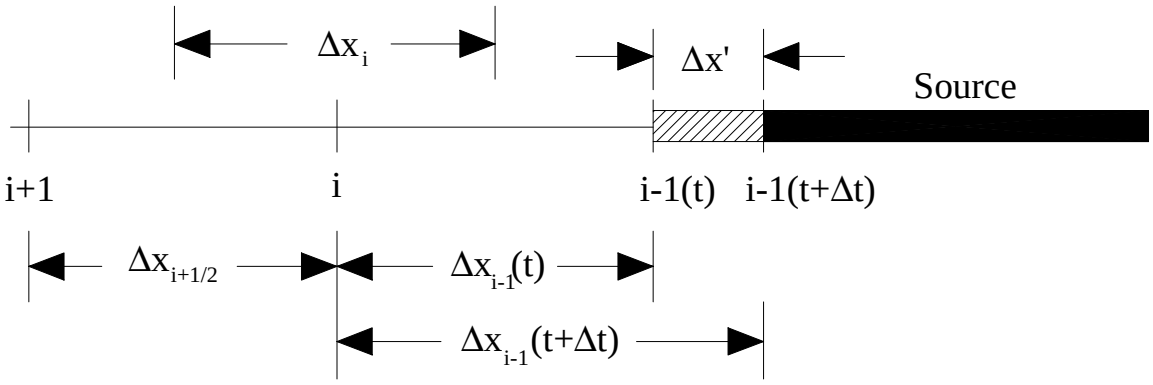

Figure 2-2. Schematic of Shrinking Source Zone.

The oil content (θ_o) in the source zone decreases also according to the dual-Monod kinetic equation which we solve again using the Runge-Kutta algorithm. For this solution we require C_o (the equilibrium concentration), to be held constant. This is due to the fact that we have a single component mixture of hydrocarbon in the source. If we were to develop a multi-component model we would have to take into account the several different equilibrium concentrations that we were modeling.

$$\left(\frac{\partial O_T}{\partial t}\right)_B = -\theta_w M_t \left(\frac{O_T}{K_{s,O_2} R_{w,O_2} + O_T}\right) F\, k_m \left(\frac{C_O}{K_s R_w + C_O}\right) = F^2 \quad (2.54)$$

$$F_1^2 = F^2(O_T) \quad (2.55)$$

$$F_2^2 = F^2\left(O_T + \frac{1}{2} h\, F_1^2\right) \quad (2.56)$$

$$F_3^2 = F^2\left(O_T + \frac{1}{2} h\, F_2^2\right) \quad (2.57)$$

$$F_4^2 = F^2\left(O_T + \frac{1}{2} h\, F_3^2 \right) \tag{2.58}$$

$$F^2(t + \Delta h) = F^2(t) + \frac{h}{6}\left(F_1^2 + 2 \cdot F_2^2 + 2 \cdot F_3^2 + F_4^2\right) \tag{2.59}$$

Since hydrocarbon and oxygen undergo biodegradation at the same time the oil content can then be found according to the equation below using the stoichiometric constant (F):

$$\Delta\theta_o = \frac{\text{hydrocarbon consumed}}{\rho_o} \tag{2.60}$$

where:

$$\text{hydrocarbon consumed} = \frac{O_2 \text{ consumed}}{F} \tag{2.61}$$

The quantity of oxygen consumed is found from the Runge-Kutta solution above (see equation 2.59).

With any numerical solution, if Δx is too large then there will exist discontinuous results. Even though $\Delta x'$ is calculated and accounted for internally, the shrinking of the source is represented in a stepwise fashion. One disadvantage of this approach is that there will be a jump in the rate of decreasing oil content. Therefore as $\Delta x'$ increases and approaches the shift in source reduction, the rate is slightly overestimated. This is discussed further in section 5.0 and Figure 5-4. This limitation can be overcome, however, by decreasing Δx, which is a minor challenge with today's computer speeds and memory capacity. For example, using 300 nodes and running the simulation for 12,000 time steps, takes about only 2-3 minutes on a Unix based server.

3.0 Validation I (Ostendorf and Kampbell 1991)

To show the significance of biodegradation as a cleanup method, we will analyze a US Coast Guard Air Station in Traverse City, Michigan, where high levels of hydrocarbon vapors throughout the vadose zone were detected and measured. In 1969, a release of more than 100,000 kg of aviation fuel entered the subsurface and currently exists as a separate phase liquid in the capillary fringe.

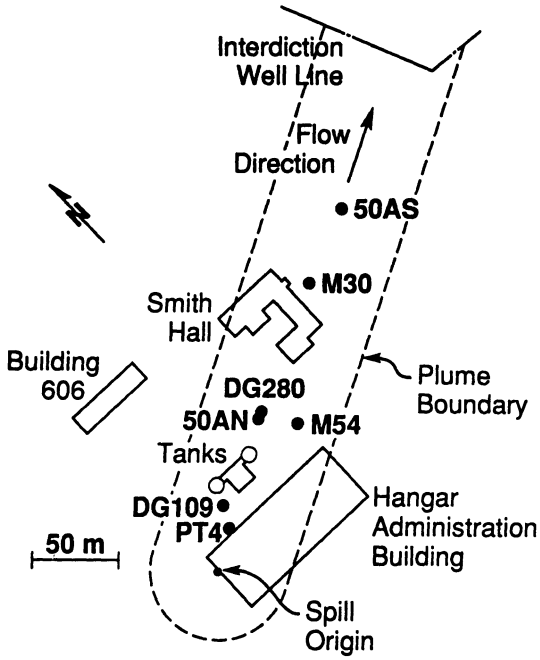

Figure 3-1. Site plan, Traverse City, Michigan (taken from Ostendorf and Kampbell, 1991).

Porosity, air and water content profiles were measured at location 50AN. The vapor concentration data was measured at locations M30 (downgradient), DG280 (near soil profile measurement), and at DG109 and PT4 (both near spill origin) as shown in Figure 3-1 above.

In 1991, the dimensions of the plume were 80 meters wide and 250 meters long and confined to a 0.3-meter thickness. There are several buildings within the area of the plume. If the vapors enter into the buildings it could pose a health threat. The water table was measured to be 5.44 meters below the soil surface. We will assume this is the top of the separate phase source (see Figure 3-2) in our simulations.

In order to simulate the data measured by Ostendorf and Kampbell (1991), we need to examine the parameters of their governing equation. The general equation used by Ostendorf and Kampbell (1991) is

$$D\frac{\partial^2 G}{\partial x^2} = V\left(\frac{G}{K+G}\right) \tag{3.1}$$

where:

D – hydrocarbon diffusion coefficient (L^2/T),
G – gaseous hydrocarbon concentration (M/L^3),
V – maximum reaction rate(T^{-1}), and
K – half saturation constant (M/L^3).

If we were to assume a uniform water content, steady state and the source being at the water table, our general governing equation (2.7) is simplified to

$$0 = D^e_w \frac{\partial^2 C}{\partial x^2} + D^e_a \frac{\partial^2 G}{\partial x^2} - \theta_w M_t k_m \left(\frac{C}{K_s + C} \right) \left(\frac{C_{O_2}}{K_{s,O_2} + C_{O_2}} \right) \tag{3.2}$$

It is believed that microbial biodegradation occurs only in the aqueous phase (Refsgaard et. al. 1991). The model of Ostendorf and Kampbell does not include the aqueous phase transport, Therefore we compare terms without the water content term. Also using Henry's Law, which is our total concentration approach without solid phase partitioning (i.e. K_d=0), we rearrange to get

$$\left(\frac{D^e_w}{H} + D^e_a \right) \frac{\partial^2 G}{\partial x^2} = \left(\frac{M_t k_m C_{O_2}}{K_{s,O_2} + C_{O_2}} \right) \left(\frac{G}{K_s H + G} \right) \tag{3.3}$$

Comparing terms in equation 3.1 and 3.3, we see the necessary correspondence as shown below:

$$D = \frac{D^e{}_w}{H} + D^e{}_a \tag{3.4}$$

$$V = \left(\frac{M_t k_m C_{O_2}}{K_{s,O_2} + C_{O_2}} \right) \tag{3.5}$$

$$K = K_s H \tag{3.6}$$

If $K_{s,O_2} << C_{O_2}$, then V becomes

$$V = M_t k_m \tag{3.7}$$

The values Ostendorf and Kampbell (1991) used from calibration and by experiment are V = 0.743 mg/L·d and K= 0.69 mg/L, based upon D = 0.208 m^2/d. The maximum reaction rate (V) used is comparable to the microcosm value obtained in the laboratory (Ostendorf and Kampbell 1990) from an unacclimated soil sample taken from the site. The half saturation constant (K) is also well represented since it's value falls within the range of observed hydrocarbon levels (Ostendorf and Kampbell 1991).

The value of K_d describes the sorption of the compound onto the soil matrix (see equation 2.14). It is found using the K_{oc} value (organic carbon) (Li and Voudrias, 1994):

$$K_d = K_{oc} \cdot f_{oc} \tag{3.8}$$

$$\log K_{oc} = 0.544 \log K_{ow} + 1.377 \tag{3.9}$$

and

$$\log K_{oc} = -0.55 \log S + 3.64 \tag{3.10}$$

where:

K_{oc} – organic carbon sorption coefficient,
f_{oc} – organic carbon content,
K_{ow} – octanol-water sorption coefficient, and
S – water solubility (mg/L).

In order to find K_{oc}, we will use the average of the previous two methods. Since there was no measurement of organic carbon content (f_{oc}), we will assume it is 1.0%, which is common for many soils (Allen-King et. al. 1996).

We will use the following parameters in our simulation:

Table 3-1. Weathered Aviation Fuel Composition and Properties[a]

Constituent	Molecular Formula	Molecular Weight	Mole Fraction[b]	Henry's Law[c]	Kow[c]	S (mg/L)[c]	D_a (m^2/d)[d]	D_w (m^2/d)[d]
2,2,4 Trimethylpentane	C_8H_{18}	114.23	21.94	124.3	12303	2.44	0.6859	9.60E-05
2,3,4 Trimethylpentane	C_8H_{18}	114.23	15.10	72.5	11220	2.3	0.6859	9.60E-05
2,3,3 Trimethylpentane	C_8H_{18}	114.23	14.33	16.8	12303	9.91	0.6859	9.60E-05
2,3 Dimethylpentane	C_7H_{16}	100.20	15.10	70.8	4265.8	5.25	0.7323	10.25E-05
2,2,5 Trimethylhexane	C_9H_{20}	128.26	8.27	99.7	38019	1.15	0.6473	9.06E-05
Toluene	C_7H_8	92.14	6.28	0.3	537.03	526	0.7637	10.69E-05
2,4 Dimethylpentane	C_7H_{16}	100.20	4.74	77.9	4265.8	5.5	0.7323	10.25E-05
2,2,3,4 Tetramethylpentane	C_9H_{20}	128.26	3.20	22.5	31623	3.87	0.6473	9.06E-05
2,3 Dimethylhexane	C_8H_{18}	114.23	3.20	15.6	13183	9.2	0.6859	9.60E-05
2,3 Dimethylbutane	C_6H_{14}	86.177	3.86	48.5	2630.3	22.5	0.7897	11.06E-05
2,5 Dimethylhexane	C_8H_{18}	114.23	2.43	20.3	13183	9.2	0.6859	9.60E-05
2,3,5 Trimethylhexane	C_9H_{20}	128.26	0.99	22.5	34674	3.59	0.6473	9.06E-05
2,2,5,5 Tetramethylhexane	$C_{10}H_{22}$	142.28	0.55	55.8	107152	1.2	0.6146	8.60E-05

[a] From Ostendorf and Kampbell (1991)
[b] adjusted mole fraction based on 100%
[c] From Howard and Meylan (1997)
[d] From Schwarzenbach et. al. (1993)

The following equation is used to find the weighted average based on the mole fraction (f_i) found in Table 3-1. For example the molecular weight is found by

$$MW = \sum MW_i \cdot f_i \tag{3.11}$$

where:

MW – average molecular weight,
MW_i –molecular weight of each compound,
f_i – mole fraction of each compound.

The other properties are found in similar fashion.

The following table shows the weighted average properties for the mixture.

Table 3-2. Properties of hydrocarbon mixture (based on mole fraction weighted average)

Molecular Weight	Henry's Law	D_a(m^2/d)	D_w(m^2/d)	Carbon	Hydrogen
110.878	67.4	0.6988	9.78×10^{-5}	7.797	17.092

From the previous table we see that the molecular formula based on a weighted average is $C_{7.797}H_{17.092}$. This will be used to find the stoichiometric constant (F) for the gasoline mixture in the following stoichiometric equation where we assume complete mineralization to carbon dioxide and water:

$$C_{7.797}H_{17.092} + 12.070\,O_2 \rightarrow 8.546\,H_2O + 7.797\,CO_2 \tag{3.12}$$

$$F = \frac{\text{mass oxygen}}{\text{mass hydrocarbon}} = \frac{12.070 \cdot 32.00}{110.878} = 3.48 \qquad (3.13)$$

where 12.070 is the O_2 coefficient necessary to balance the above stoichiometric equation, 32.00 is the molecular weight of oxygen, and 110.878 is the average molecular weight of the gasoline mixture. The number of moles is one.

It is assumed that there exists a steady state microbial community with negligible sloughing of biomass. This assumption is valid considering the prolonged presence of hydrocarbon vapors over the 30-year life of the plume. The then present conditions reflect an equilibrium between the biological and diffusive processes.

Table 3-3. Numerical Parameters.

Name	**Value (common units)**	**(SI Units)**
ω (weighting factor)	1.0 (fully implicit)	1.0
Δt	2 days	2 days
Δx	0.02 m	0.02 m
Length of zone (L_2)[a]	5.44 m	5.44 m

[a] From Ostendorf and Kampbell 1991
[b] From Henry's Law: equation 2.15
[c] we assume atmospheric conditions of 21% oxygen (units converted using the Ideal Gas Law)
[d] below which no degradation takes place

Table 3-4. Parameters of Monod Kinetics.

Name	**Value (common units)**	**(SI Units)**
microbial cell concentration (M_t)[a]	0.23 mg/L	0.00023 kg/m^3
maximum utilization rate (k_m)[b]	3.23 day^{-1}	3.23 day^{-1}
half saturation constant (hydrocarbon) (K_s)[c]	0.13 mg/L	0.00013 kg/m^3
half saturation constant (oxygen) (K_{s,O_2})[c]	0.1 mg/L	0.0001 kg/m^3
utilization ratio (F)[d]	3.48	3.48

[a] From MacQuarrie et. al. (1990)
[b] From equation 3.7
[c] From Borden and Bedient (1985)
[d] From equation 3.13

Only the product of M_t and k_m is being compared here. Hence we will use the value of 0.23 mg/L as the microbial cell concentration (estimated by MacQuarrie et. al. 1990) and the value of k_m then is determined from equation 3.7.

Table 3-5. Physical Parameters.

Name	Value (common units)	(SI Units)
vapor diffusion of hydrocarbon (D_a)[a]	0.6988 m^2/d	0.6988 m^2/d
vapor diffusion of oxygen (D_{a,O_2})[b]	1.6857 m^2/d	1.6857 m^2/d
aqueous diffusion of hydrocarbon (D_w)[a]	$9.78x10^{-5}$ m^2/d	$9.78x10^{-5}$ m^2/d
aqueous diffusion of oxygen (D_{w,O_2})[b]	$18.14x10^{-5}$ m^2/d	$18.14x10^{-5}$ m^2/d
hydrocarbon equilibrium conc. in vapor phase[a]	146 mg/L	0.146 kg/m^3
initial oxygen conc. in water phase[b]	9.28 mg/L	0.00928 kg/m^3
initial oxygen conc. in vapor phase[c]	287 mg/L	0.287 kg/m^3
hydrocarbon cut off concentration in water phase[d]	0.1 mg/L	0.0001 kg/m^3
oxygen cut off concentration in water phase	1.0 mg/L	0.001 kg/m^3
temperature	285 K	12 °C
Henry's Law constant (hydrocarbon)[a]	67.4	67.4
Henry's Law constant (oxygen)[c]	30.94	30.94
K_d (hydrocarbon)[d]	29.32 L/kg	0.02932 m^3/kg
bulk density (ρ_b)	1.6 kg/L	1600 kg/m^3

[a] From Table 3-2
[b] From Schwarzenbach et. al. (1993)
[c] From Lyman (1990)
[d] From equations 3.8, 3.9, and 3.10

In order to clarify any misunderstanding, our simulation is not under steady state conditions as the Ostendorf model is. We are concerned with validating our governing equations, (2.16) and (2.23), using data they measured, and not applying their model.

Based on the site temperature and atmospheric pressure, the initial and boundary conditions for oxygen are

$$@\, t = 0 \qquad C_{O_2} = 9.28\ mg/L \quad (aq) \tag{3.15}$$

$$@\, x = 0 \ \text{(surface)} \qquad C_{O_2} = 9.28\, mg/L\, (aq) \tag{3.16}$$

$$@\, x = L \ \text{(gw table)} \qquad \frac{\partial O_T}{\partial t} = 0 \tag{3.17}$$

The boundary conditions used by Ostendorf at the groundwater table is a Type I constant concentration of 0 mg/L. If there was no depletion of oxygen due to degradation, we would see that the oxygen vapor concentration would completely fill the pore space and reach atmospheric conditions. By forcing the concentration to be zero at the water table, they are forcing a linear relationship from atmospheric conditions at the surface to 0 mg/L at the water table. Type II boundary conditions of no flow for the oxygen is more realistic. The reason for depletion of oxygen near the water table is due to hydrocarbon vapors being present and the biodegradation process occurring. Since the hydrocarbon source is located at the water table, we leave out Zone III from Figure 1-2 as shown in Figure 3-2.

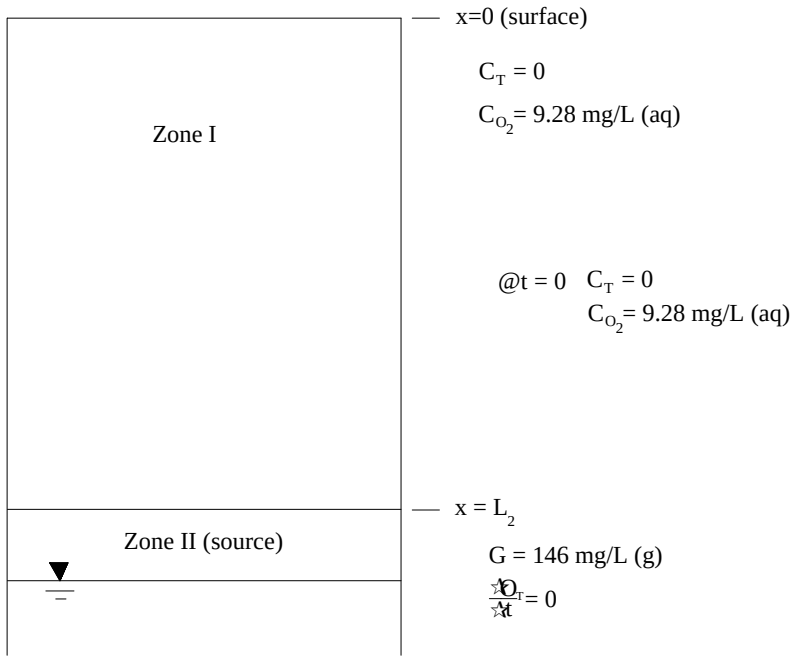

Figure 3-2. Ostendorf and Kampbell scenario.

The initial and boundary conditions for the hydrocarbon are

$$@\,t = 0 \qquad C_T = 0 \tag{3.18}$$

$$@\,x = 0 \ \text{(surface)} \qquad C_T = 0 \tag{3.19}$$

$$@\,x = L \ \text{(gw table)} \qquad G = 146\ \text{mg/L (g)} \tag{3.20}$$

The value of 146 mg/L is taken from Ostendorf and Kampbell (1991) and represents the average vapor pressure of the hydrocarbon mixture of Table 3-1.

In Figure 3-3 we show the measured data. As noted earlier there are 4 locations where vapors were measured. The key location is DG280 (see Figure 3-1) which also has porosity and air & water content measurements within close proximity. In Figure 3-3 the data points show the actual hydrocarbon concentration data values. The lines show the average for each of the 4 locations. The data set that we will try to model is the one near the measured soil profile. The other data is included to provide discussion later.

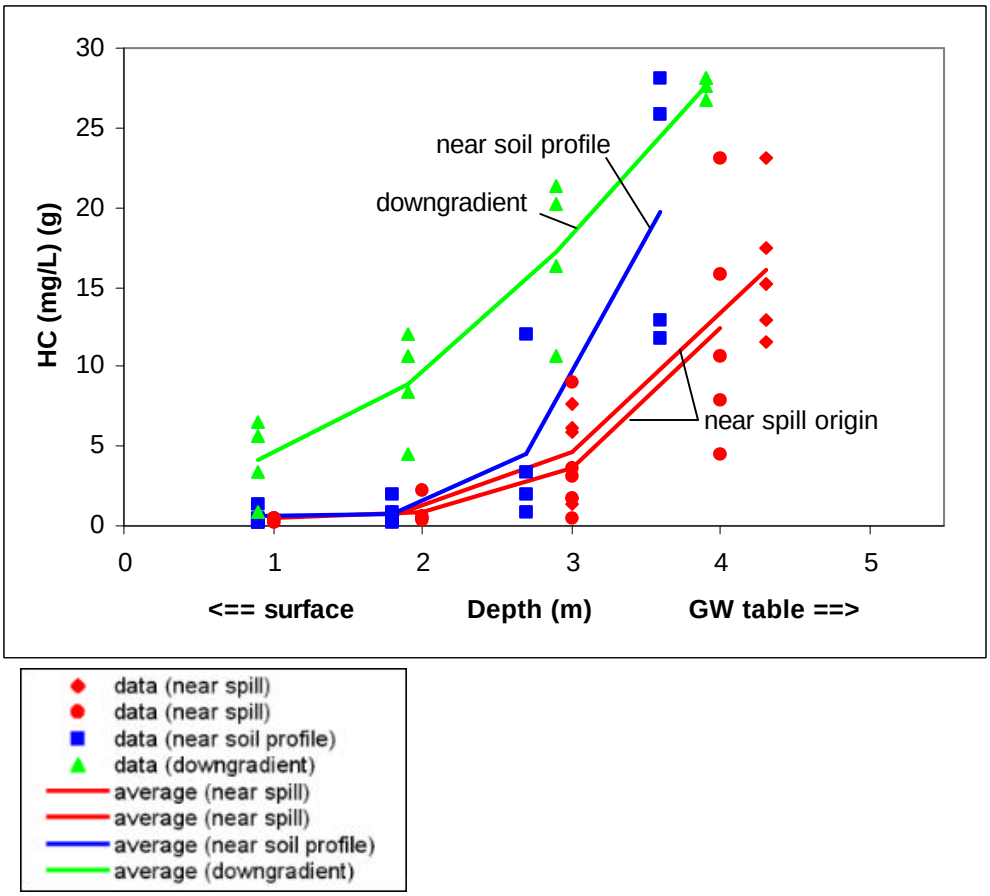

Figure 3-3. Measured hydrocarbon data from Traverse City, Michigan.

We have the measured moisture content profile in Figure 3-4 taken from location 50AN (see Figure 3-1). One advantage of numerical modeling is that we can simulate the diffusion process with a changing air content. As will be shown later, this has a significant affect on the outcome since the diffusion coefficient is a function of the air content (see equation 2.4).

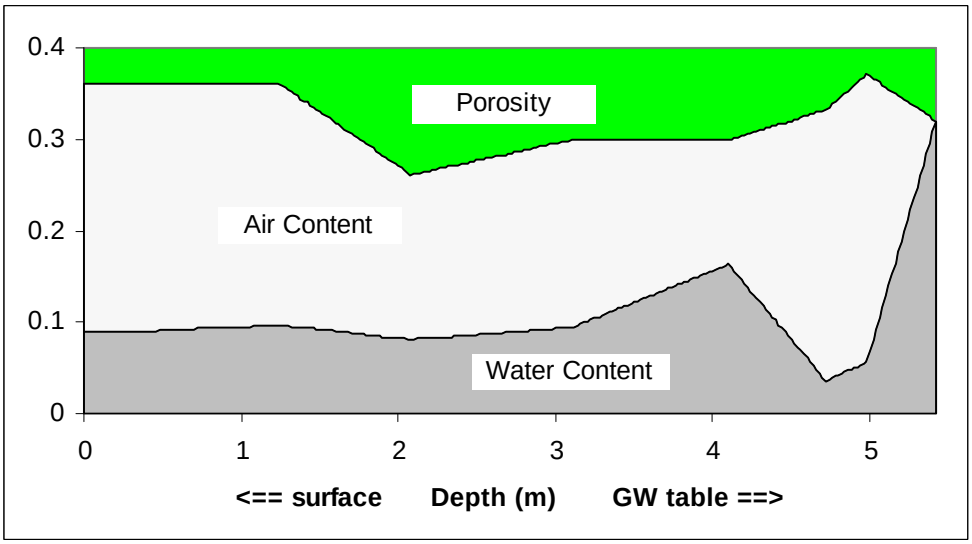

Figure 3-4. Moisture content profile.

The data measured for the porosity and air content consists of 8 point measurements at different depths. The water content then is calculated by subtracting the two concentrations. The values in between the depths are assumed to follow a linear relationship from point to point.

Results

First we will look at a case where no degradation is involved. This will allow us to look at how the diffusion coefficient influences the transport without the degradation term in equation 2.7. From the dark line in Figure 3-5, it shows that hardly any hydrocarbon vapors leave the water table area. This is due to the extreme low diffusion coefficient caused by the small air content near the boundary. These plots show the steady state results.

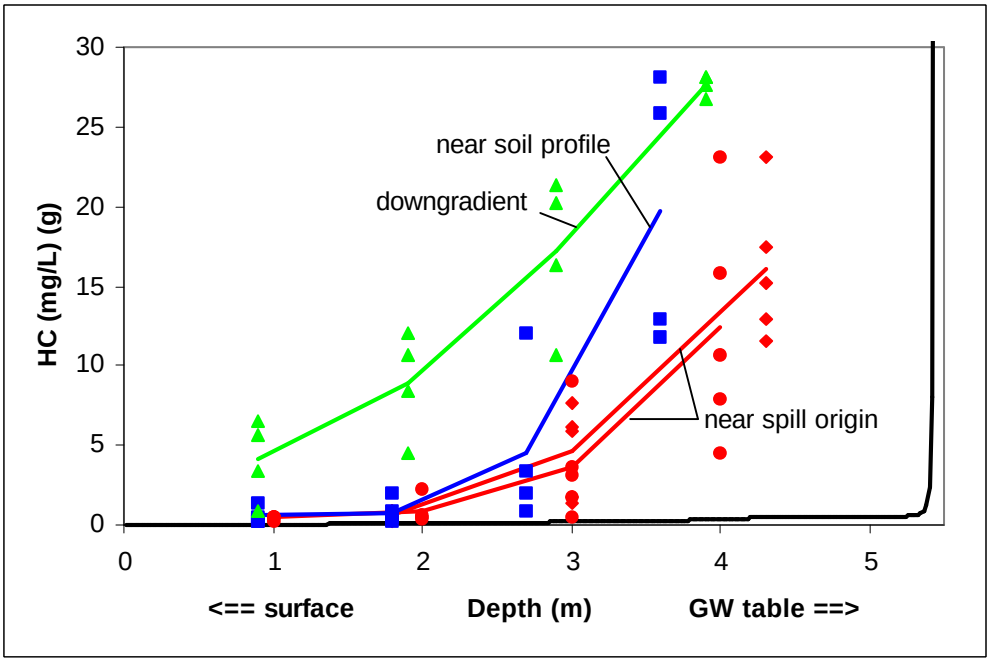

Figure 3-5. Concentration results compared to field data (no degradation).

From equation 2.4, we see that due to the small air content near the water table that the diffusion coefficient for the hydrocarbon is very small. This explains the low results in Figure 3-5.

Since the water table is constantly fluctuating from season to season and to a lesser extent from storm to storm, we can adjust the moisture content near the boundary and explore other possible scenarios.

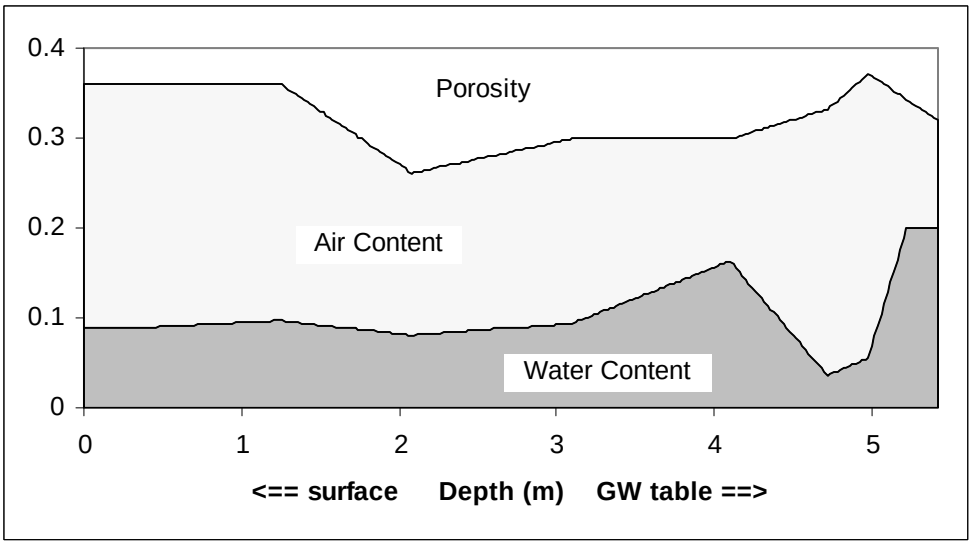

Figure 3-6. Adjusted moisture content profile.

Here we adjust the water content, and hence the air content, near the boundary as shown in Figure 3-6.

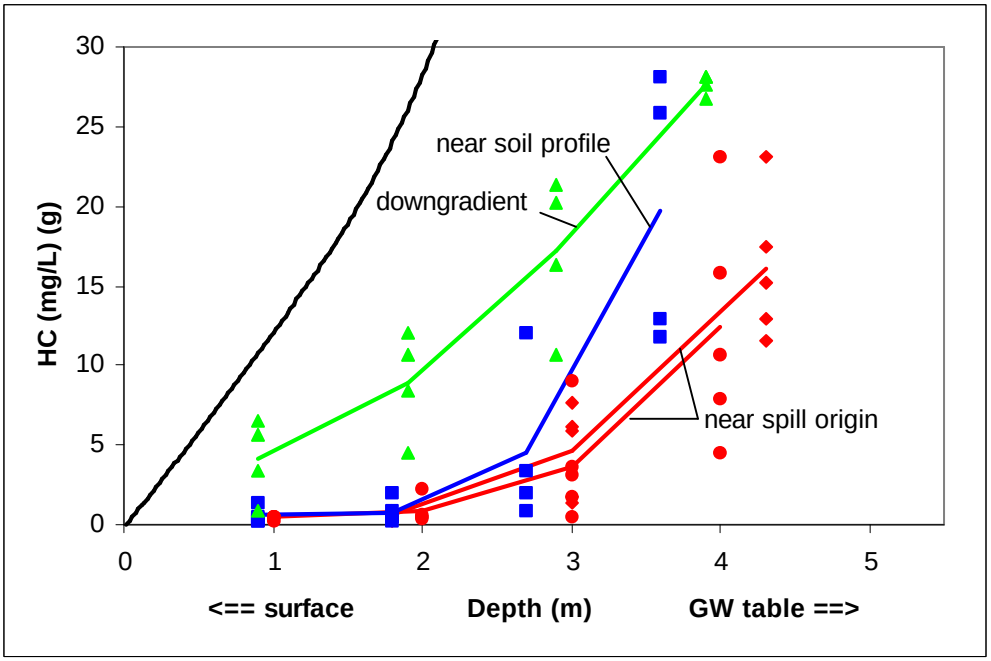

Figure 3-7. Concentration results compared to field data (no degradation)(based on Figure 3-6 soil profile).

In Figure 3-7, we see that the vapor concentrations are higher than the measured values. The amount we adjusted the moisture profile may be extreme unless there is an excessive rise in the water table, so we will try another adjustment as shown in Figure 3-8.

.

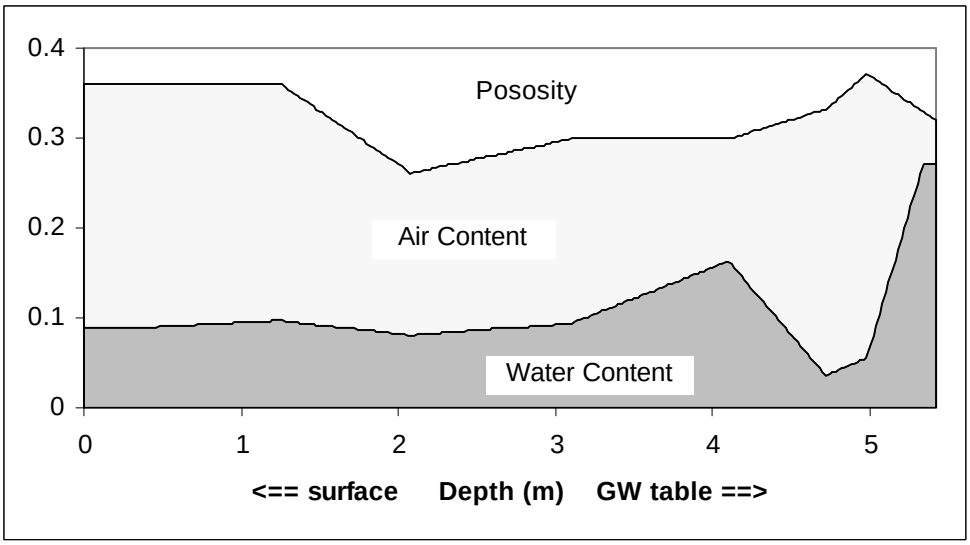

Figure 3-8. Adjusted moisture content.

In Figure 3-9 we get vapor concentrations that closely match the upper limit of measured data. Keep in mind that this is without degradation. Once we add the biodegradation we will see even lower values as desired.

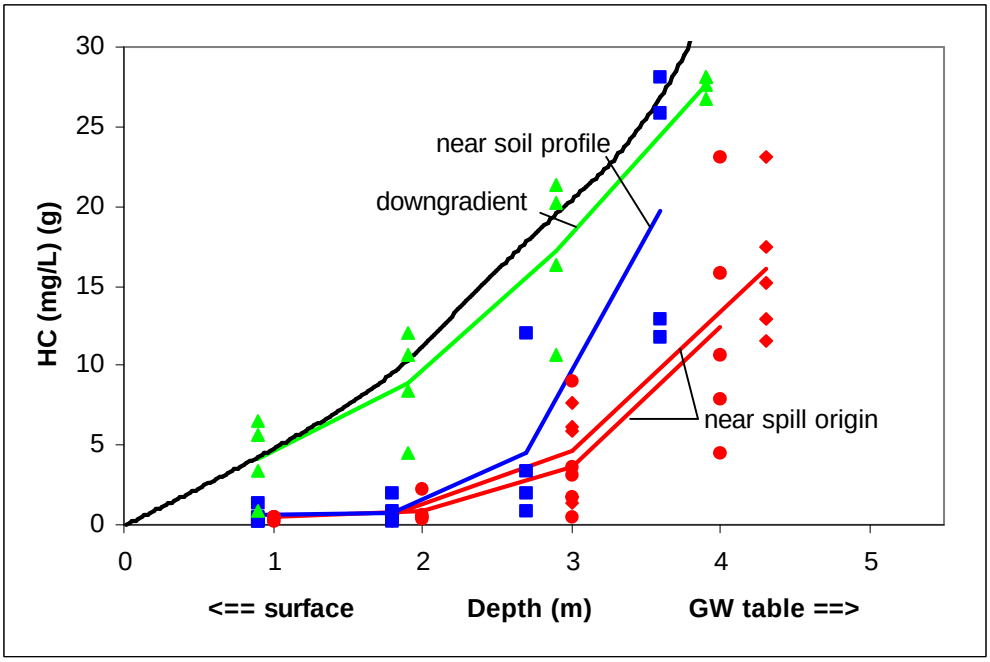

Figure 3-9. Concentration results (no degradation) (based on Figure 3-8 soil profile).

If we use the moisture content as adjusted in Figure 3-8, and allow degradation to take place, we get the results as plotted in Figure 3-10.

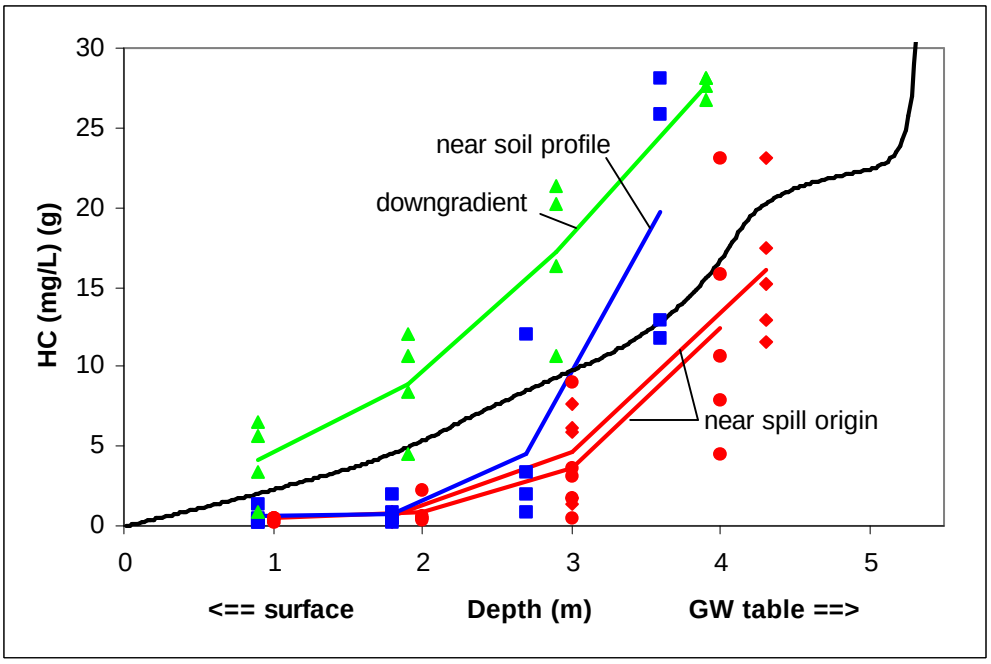

Figure 3-10. Concentration results (with degradation see Table 3-6 Scenario #8) (based on moisture content profile from Figure 3-8)

As seen above, we can adjust the moisture content to get the results we want. This shows the sensitivity of the diffusion coefficient as a function of air content. During dry conditions we will see large contamination potential compared to wet conditions. By keeping the soil wet may prove to be a remediation option for hydrocarbon vapors near enclosed spaces that pose a health threat. However too much infiltration of water will lead to a raise in the water table which causes the separate phase to rise as well. We can see very clearly that a minor change in water content near the water table can cause a major change in concentration results.

We will now run a sensitivity analysis on the Monod parameters to see how they influence the simulation. In Figure 3-11 and Table 3-6, we see 10 different scenarios. The first 3 were taken from Figures 3-5, 3-7 and 3-9 where no degradation is involved. While #8 is the same as shown in Figure 3-10. The others test the sensitivity of the half saturation constants for the hydrocarbon (K_s) pseudo-compound and oxygen (K_{s,O_2}), and also the maximum utilization rate (k_m). The half saturation constants are defined as the the concentration at which the utilization rate is half the maximum. The scenarios #3 through #10 are based on the moisture content adjusted in Figure 3-8.

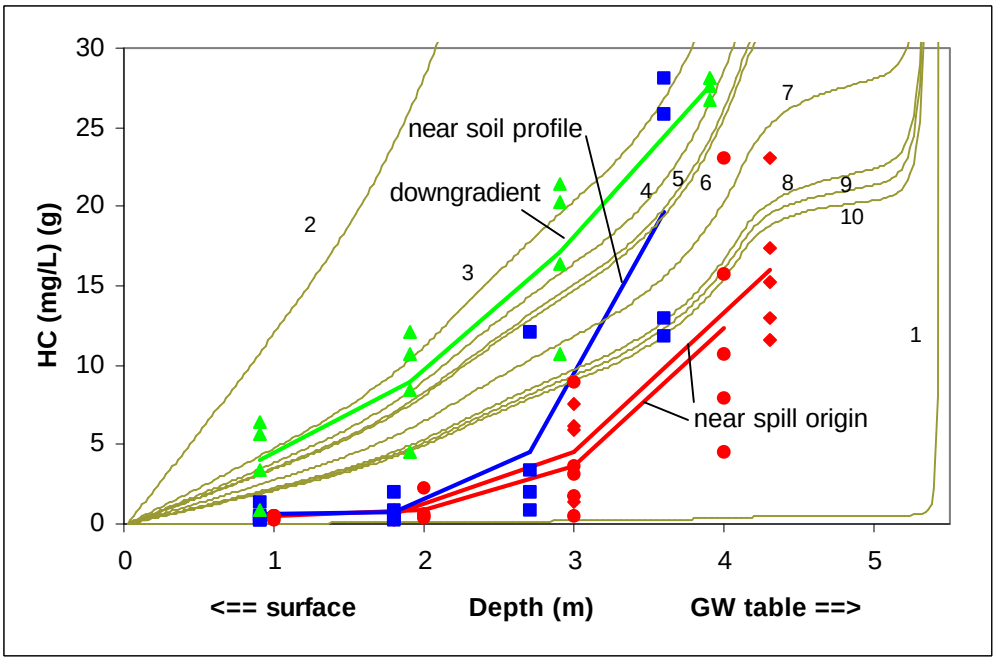

Figure 3-11. Summary of results (see Table 3-6).

Table 3-6. Sensitivity Analysis.

Scenario	k_m	K_s	K_{s,O_2}
1	no degradation		
2	no degradation (adjusted moisture content see Fig 3-6)		
3	no degradation (adjusted moisture content see Fig 3-8)		
4	0.493[a]	0.13[c]	0.1[a,c]
5	3.23[b]	2.0[d]	1.0[d]
6	3.23	2.0	0.1
7	3.23	0.65[a]	0.1
8	3.23	0.13	0.1
9	4.0[d]	0.13	0.1
10	7.0	0.13	0.1

[a] From MacQuarrie et. al. (1990)
[b] From Ostendorf and Kampbell (1991)
[c] From Borden and Bedient (1985)
[d] From Semprini et. al. (1991)

Since we are trying to fit the vapor data where the soil moisture was measured, we will explore further into the sensitivity of other parameters. One advantage of modeling the past data is that we know what the results should be (compared to predicting the future which is unknown). If we modify applicable parameters we can get a sense of how the model works. The first is the Boundary Condition concentration for oxygen near the surface. Previously we have used atmospheric conditions, which are normally about 9.3 mg/L in the aqueous phase. If we look at the data measured at 1-meter depth, we see a oxygen concentration of 3.3 mg/L (aq). To use this value as our BC, we can assume depletion due to vegetation and/or other microbiological processes (other than hydrocarbon degradation) near the soil surface as well as mass transfer limitations due to compaction of soil. Further investigation is necessary to substantiate this assumption.

Another modification we can use to reach a better fit is by looking at the moisture content profile. It is possible to conclude that the moisture content profile was not measured at the same time as the vapor contamination concentrations. We can therefore adjust the moisture accordingly. From Figure 3-8, we see

a high moisture content zone or hump near the 4-meter depth. This yields a small air content which greatly affects the diffusion coefficient according to equation 2.4. If we shift this upward to about 3.6 meters, we see hydrocarbon concentrations results closer to the field data.

Figure 3-12 shows a modified soil profile with the water content hump shifted upwards about 40 cm.

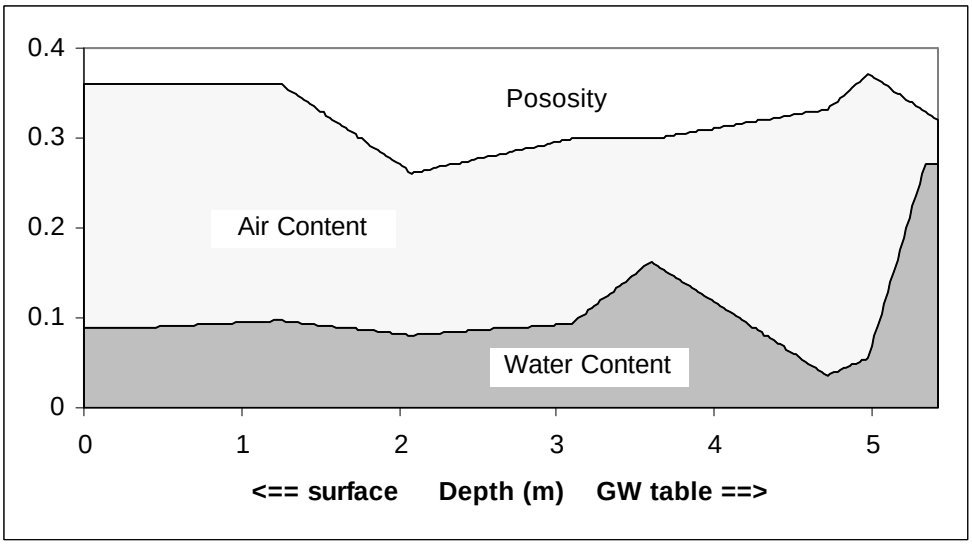

Figure 3-12. Modified soil profile.

By including the oxygen data measured at the site, we see that more degradation must take place to allow hydrocarbon concentrations and oxygen concentrations to match the field data. We can also adjust the Monod kinetics parameters. The stoichiometric constant (F) does have a significant effect on the results. Since there are many compounds in a gasoline mixture, it is valid to increase F to compensate for the compounds not being included in our simulation. We are simulating one hydrocarbon compound or pseudo-compound described by the mixture of Table 3-1.

Figure 3-13 shows several time series associated with the simulation described in Table 3-7. The field data shown are the point averages coordinating to the dark average lines of Figure 3-3 for the location near the soil profile measurements.

Not included here is data measured for oxygen similar to Figure 3-3 which were taken at the same time as a the hydrocarbon concentrations. Again the points in Figure 3-13 correspond to average oxygen concentration values at the location near the measured soil profile.

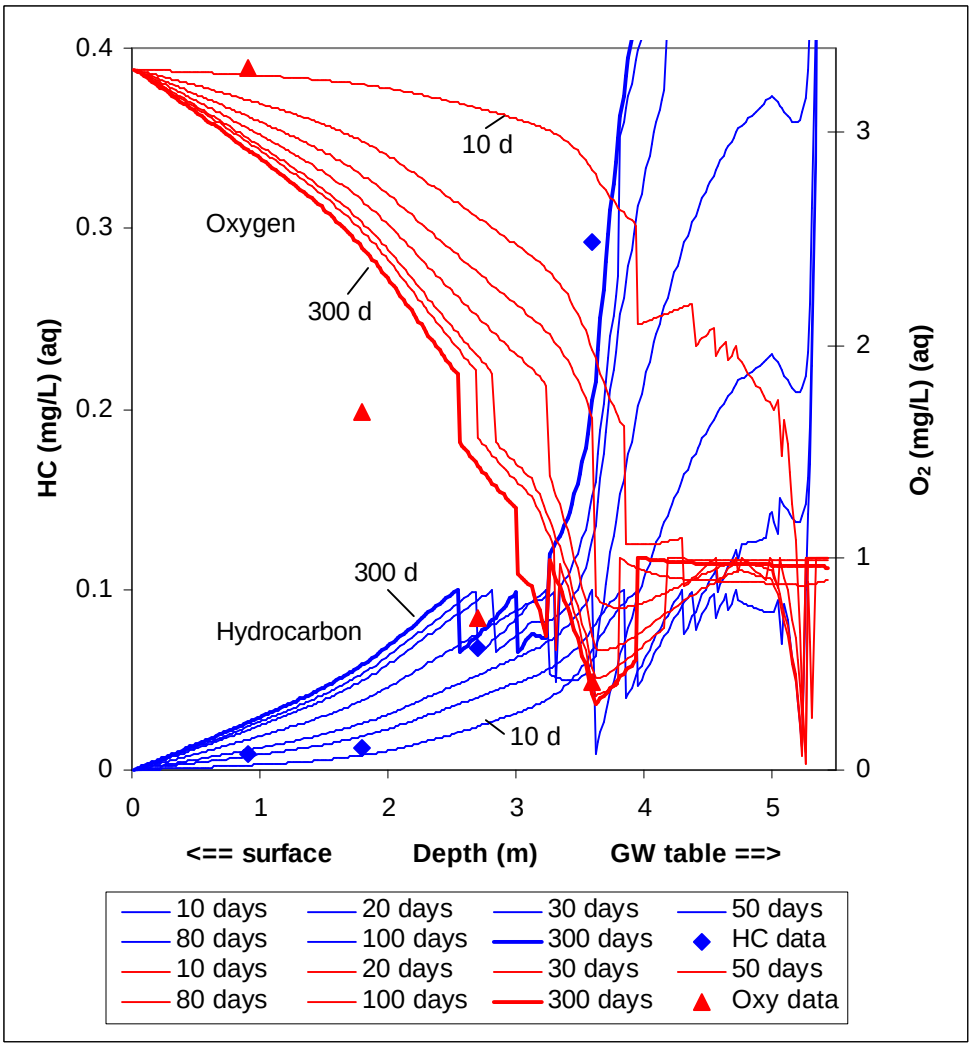

Figure 3-13. Concentration results.

The above field data are the averages at site DG280 which is very near site 50AN where the porosity and air content data were measured. Note that in order to take a closer look at the effect the hydrocarbon cut off concentration has on the simulation, we have converted the hydrocarbon concentration to the aqueous phase for Figure 3-13. It is common that biodegradation does not occur when the oxygen concentration falls below 1.0 mg/L (aq). If we were to increase the cut off value for the hydrocarbon, we would see a better fit near the surface.

We can increase the hydrocarbon equilibrium concentration, since the water table fluctuates and exposes the source to air filled pore space. This is one to way to overcome the mass transfer limitations noted by Ostendorf and Kampbell (1991) in the capillary fringe. The parameters that were adjusted to get this fit are shown below:

Table 3-7. Fitting Parameters.

Name	**Value (common units)**	**(SI Units)**
oxygen concentration at the surface (BC)[a]	3.3 mg/L	0.0033 kg/m^3
hydrocarbon equilibrium conc. in vapor phase[b]	250 mg/L	0.250 kg/m^3
maximum utilization rate (k_m)	15 day^{-1}	15 day^{-1}
utilization ratio (F)	4	4
half saturation constant (hydrocarbon) (K_s)[b]	0.01 mg/L	0.00001 kg/m^3

[a] due to possible depletion from vegetation and other microbial processes
[b] increased to compensate for mass transfer limitations in the capillary fringe
[b] From Ostendorf and Kampbell (1991) and equation 3.6

Discussion

The concentration of hydrocarbon and oxygen vapors were detected in the unsaturated zone above the contaminated capillary fringe from an aviation gasoline spill at the U.S. Coast Guard Air Station in Traverse City, Michigan. The subsequent numerical analysis was developed based on two general governing equations 2.16 and 2.23. This analysis proceeds under the absence of advection, which is based on the absence of any gradients, which may cause advection. We also assume the complete mineralization to carbon dioxide and water of the gasoline mixture and the oxygen present.

From Figures 3-5, 3-7, and 3-9, we see that the hydrocarbon concentrations are quite sensitive to the air content. An accurate air content profile is almost essential in fitting the data to the model. The sensitivity of equation 2.4 is obvious, especially near the water table where the air content is very small. Since the water table fluctuates and exposes the source to air filled pore space, vapors are then released and diffuse at a much higher rate than when conditions of near saturation exist at the source boundary. More detailed data such as simultaneous measurements of air content and vapor concentrations near the water table would be useful in providing a better understanding of diffusion transport.

In future modeling efforts, we could develop a multiple component model and include advection due to any density gradients that arise due to differences in partitioning coefficients for each constituent. Density gradients would exist if we were to develop a multi-component model (Falta et. al. 1989). Under these circumstances a pattern may emerge similar to a Gas Chromatograph analysis in the laboratory. The compound with the least affinity for the porous medium is least retarded and hence will appear on the leading edge of the plume (Hinchee and Reisinger 1985).

Also from Kampbell et al. (1990) carbon dioxide concentrations at Traverse City were measured, which could be considered in light of the stoichiometry assumption of complete mineralization.

Since the diffusion process is unaffected by gravity, the vapors diffuse radially and not just in the vertical direction. This is a possible explanation for the higher hydrocarbon concentrations downgradient (see Figure 3-3). This can also lead to vapors up gradient as well which can lead to a miss-representation of the source location if the source was small in length. Since this plume is over 250 m in length, it is expected that higher concentrations of vapors are detected near the center of the plume which is near to location M30 (see Figure 3-1).

The sensitivity of the diffusion coefficient to the air content near the water table cannot be over emphasized. With the increased use of risk-based decision making and RBCA, it is becoming clear that In Situ measurements of diffusion coefficients are necessary (Johnson et. al. 1998).

4.0 Validation II (Fischer et al. 1996)

The second site where we want to demonstrate the significance of biodegradation consists of a former gasoline station located at the Alameda Naval Air Station in California. In 1980, one of the three underground storage tanks was damaged and assumed repaired. In 1988 it was determined that a problem still existed and the fuel in the tanks was removed and the station was closed. In 1990, there were still high concentrations of hydrocarbon vapors detected in the soil, and trace amounts found in the building itself , the highest of which was Isopentane (0.026 μg/L). The service station building is a one-story building with a floor area of approximately 50 m^2.

Unlike the previous validation, the depth to the water table is only 1.92 meters.

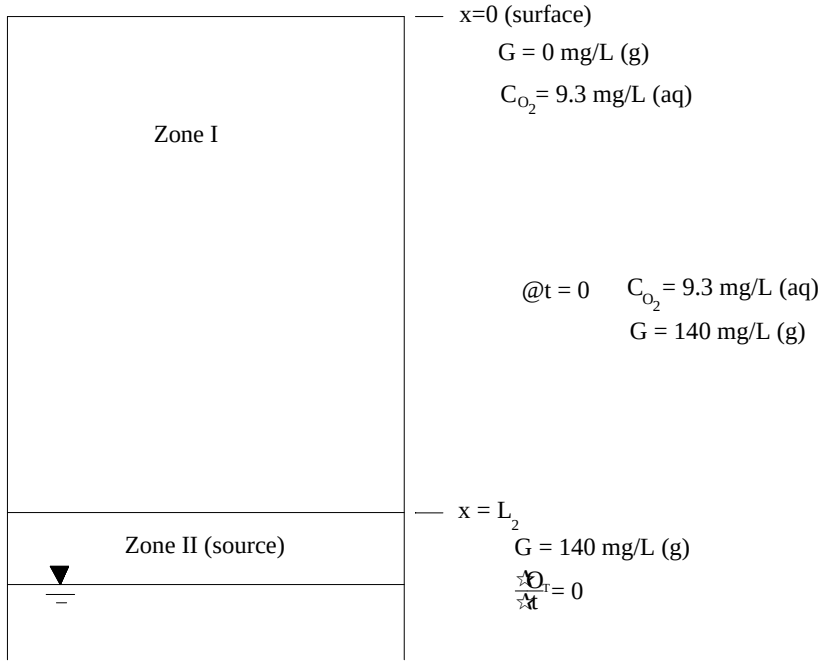

Figure 4-1. Fischer scenario.

Based on the site temperature and atmospheric pressure, the initial and boundary conditions for oxygen are

$$@\,t = 0 \qquad C_{O_2} = 9.3\,mg/L\,(aq) \tag{4.1}$$

$$@\,x = 0 \ \text{(surface)} \qquad C_{O_2} = 9.3\,mg/L\,(aq) \tag{4.2}$$

$$@\,x = L \ \text{(gw table)} \qquad \frac{\partial O_T}{\partial t} = 0 \tag{4.3}$$

Since the hydrocarbon source is located at the water table, we are only interested in Zone I (Figure 1-2). The initial and boundary conditions for Isopentane are

$$@\,t = 0 \qquad G = 140\,mg/L\,(g) \tag{4.4}$$

$$@\,x = 0 \ \text{(surface)} \qquad G = 0\,mg/L\,(g) \tag{4.5}$$

$$@\, x = L \ \text{(gw table)} \qquad G = 140\ \text{mg/L (g)} \tag{4.6}$$

The value of 140 mg/L is the vapor pressure of Isopentane based on the site temperature and pressure. The initial conditions are set to 140 mg/L as well to see how the simulation progresses initially compared to when a clean vadose zone IC (G=0 mg/L) is set. Both result in the same end steady state outcome.

Even though the indoor air concentration has been measured, we have set the boundary condition at the surface to 0 mg/L. The vapor flux entering the building is calculated using the difference in the last two nodal concentration values (i.e. the concentration gradient). A ventilation procedure is implemented to determine the concentration of vapors that pose hazardous health threats. If there was no ventilation in the building, the concentration would continue to increase. Since we know the indoor air concentration, we can back calculate using the flux that we determine from simulation and find the ventilation algorithm that links the in-flux to the air concentration.

The stoichiometric constant for Isopentane is found by

$$C_5H_{12} + 8\,O_2 \rightarrow 6\,H_2O + 5\,CO_2 \tag{4.7}$$

$$F = \frac{\text{mass oxygen}}{\text{mass hydrocarbon}} = \frac{8 \cdot 32.00}{72.15} = 3.55 \tag{4.8}$$

where 72.15 is the molecular weight of C_5H_{12} (Isopentane). The parameters used in this simulation are given in the next table:

Table 4-1. Numerical Parameters.

Name	**Value (common units)**	**(SI Units)**
Δt	2 days	2 days
Δx	0.02 m	0.02 m
Length of zone (L_2)[a]	1.92 m	1.92 m

[a] From Fischer et. al. (1996)
[b] From Henry's Law: equation 2.15
[c] we assume atmospheric conditions of 21% oxygen (units converted using the Ideal Gas Law)

Table 4-2. Parameters of Monod Kinetics.

Name	**Value (common units)**	**(SI Units)**
microbial cell concentration (M_t)[a]	0.23 mg/L	0.00023 kg/m^3
maximum utilization rate (k_m)[b]	6.8 day^{-1}	6.8 day^{-1}
half saturation constant (hydrocarbon) (K_s)[a]	0.65 mg/L	0.00065 kg/m^3
half saturation constant (oxygen) (K_{s,O_2})[a]	0.1 mg/L	0.0001 kg/m^3
utilization ratio (F)[c]	3.55	3.55

[a] From MacQuarrie et. al. (1990)
[b] From Tabak (1991)
[c] From equation 4.8

Table 4-3. Physical Parameters.

Name	**Value (common units)**	**(SI Units)**
vapor diffusion of Isopentane (D_a)[a]	0.863 m^2/d	0.863 m^2/d
aqueous diffusion of Isopentane (D_w)[a]	0.0001208 m^2/d	0.0001208 m^2/d
vapor diffusion of oxygen (D_{a,O_2})[a]	1.6857 m^2/d	1.6857 m^2/d
aqueous diffusion of oxygen (D_{w,O_2})[a]	0.0001814 m^2/d	0.0001814 m^2/d
Isopentane equilibrium conc. in air phase[a]	140 mg/L	0.140 kg/m^3
Isopentane indoor vapor conc.[a]	0.026 µg/L	0.000000026 kg/m^3

initial oxygen conc. in water[b]	9.28 mg/L	0.00928 kg/m^3
initial oxygen conc. in air[c]	287 mg/L	0.287 kg/m^3
hydrocarbon cut off concentration in water phase	0.1 mg/L	0.0001 kg/m^3
oxygen cut off concentration in water phase	1.0 mg/L	0.001 kg/m^3
Henry's Law constant (Isopentane)[b]	55.77	55.77
Henry's Law constant (oxygen)[c]	30.94	30.94
K_d (Isopentane)[d]	1.89 L/kg	0.00189 m^3/kg
bulk density (ρ_b)	1.55 kg/L	1550 kg/m^3

[a] From Schwarzenbach et. al. (1993)
[b] From Howard and Meylan (1997)
[c] From Lyman (1990)
[d] From equations 3.8, 3.9, and 3.10

The porosity and water & air contents were measured at 11 different depths. Table 4-4 and Figure 4-2 both show the corresponding data. It should be noted that the sampling resolution for this second validation is much smaller.

Table 4-4. Physical Properties of Soil (field data).

Depth (m)	Porosity	Water content	Air content	Bulk Density	Organic Carbon
0.20	0.37	0.13	0.24	1.6	0.4
0.38	0.37	0.14	0.23	1.6	0.3
0.48	0.33	0.12	0.21	1.7	0.1
0.58	0.38	0.17	0.21	1.6	0.4
0.62	0.39	0.20	0.19	1.5	0.5
0.70	0.34	0.18	0.16	1.6	0.6
0.95	0.39	0.13	0.26	1.6	0.07
1.14	0.38	0.12	0.26	1.6	0.06
1.35	0.41	0.15	0.26	1.5	0.06
1.60	0.46	0.28	0.18	1.4	0.08
1.96	0.51	0.43	0.08	1.3	0.07

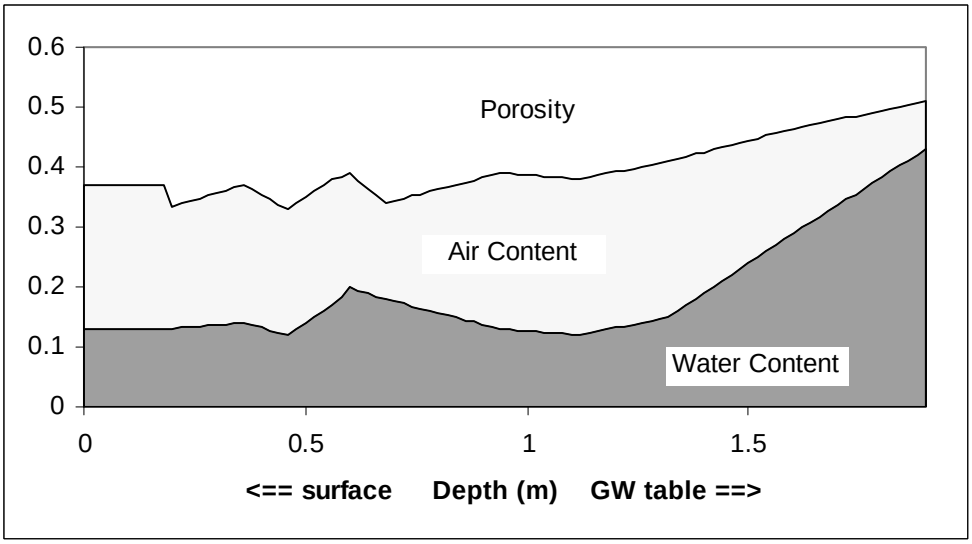

Figure 4-2. Profile of Soil (field data).

Again we assume a linear relationship between porosity and air content, which is less significant than the first validation, since this data set is more refined.

Figure 4-3 shows a complex sensitivity analysis on 3 parameters. The first parameter is the BC concentration at the source for the hydrocarbon. The second is the maximum utilization rate (k_m). And the third is the utilization ratio (F). Each data series represents steady state.

Table 4-5. Sensitivity Analysis Parameters

Parameter	Hydrocarbon BC concentration (mg/L) (g)	maximum utilization rate (k_m)	utilization ratio (F)
A	140	6.8	3.55
B	250	6.8	3.55
C	500	6.8	3.55
D	140	30	3.55
E	140	60	3.55
F	140	60	10
G	140	60	15
H	250	60	15
I	500	60	15

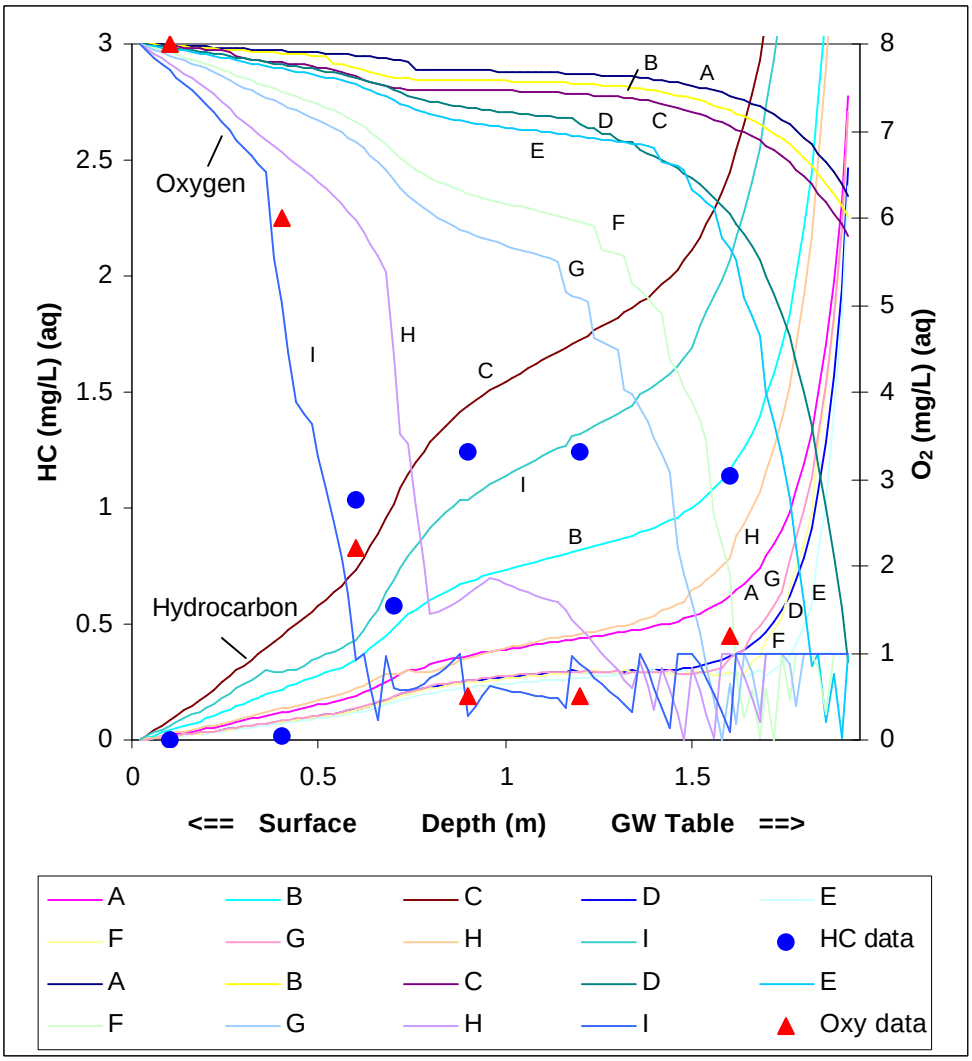

Figure 4-3. Sensitivity Analysis Results.

The first 3 scenarios (A, B, & C) show how the BC affects the simulation. There is little change in the oxygen values, but a significant difference in the hydrocarbon values. The next set (A, D & E) show how the maximum utilization rate (k_m) affect the simulation. There seems to be only a slight difference for either oxygen or hydrocarbon, but the change is consistent with the increasing k_m. If we look at E, F & G, we see how the utilization ratio (F) affects the simulation. Here both the hydrocarbon and the oxygen change very little , but is consistent with the increasing F. The final 3 (G, H, & I) match the corresponding data well. Here we change the BC and see results that fit the data quite well.

The oscillations of oxygen near the water table is due to the nature of numerical solutions. With the cut off concentration for oxygen at 1 mg/L we see the concentrations oscillating at these low values. The reduction of oxygen due to biodegradation may overshoot the cut off concentration set and would then be reset back to the 1 mg/L. Diffusion would also adjust these concentrations as well.

Discussion

We note the possibility of mass transfer limitations within the contaminated capillary fringe (Pfannkuch 1984). This may explain why the model does not match the data near the water table. Also as noted by Fischer et al. (1996), there exists a low-diffusivity layer between 0.4 and 0.65 meters. They claim this causes the field data gradients shown in the previous plots. Since the water content within this zone is high causing a lower air content, the resulting diffusion coefficient is in fact much less (as described in equation 2.4).

It should be noted that the depth to the water table after a series of heavy rainfall was once measured to be only 1.0 meters below the soil surface. This could explain how vapors of higher concentration than predicted reached such a height as measured in the field, since residual vapors could have been exposed to depths near here.

One of the main reasons for including the aqueous phase diffusion is the fact that near the water table the vapor pore space is small and the water content is near the porosity value. Under these conditions the aqueous diffusion process becomes more significant than usual, while the vapor diffusion process becomes less dominant.

The actual composition of the vapors measured in the field show several compounds including isopentane. We choose isopentane because it had the highest vapor concentration in the building (i.e. the surface). If we were to include all the compounds and develop a multi-compound model, we could keep track of the changing composition of the separate phase source.

Also near the surface, oxygen can be depleted by consumption from vegetation in the root zone and consumption due to other microbial activity not related to petroleum hydrocarbons. Thus a complete accounting should include two thin layers adjacent to the ground surface and the water table. More detailed field data is necessary for this simulation to be more useful.

5.0 Separate Phase Example

We now look at an example where the contamination is located above the water table as a separate phase liquid where we have unsaturated soil above and beneath the source zone. The purpose of this example is to quantify the contamination potential to the surface and to the groundwater. It is also desired to determine the source longevity as described in section 2.0.

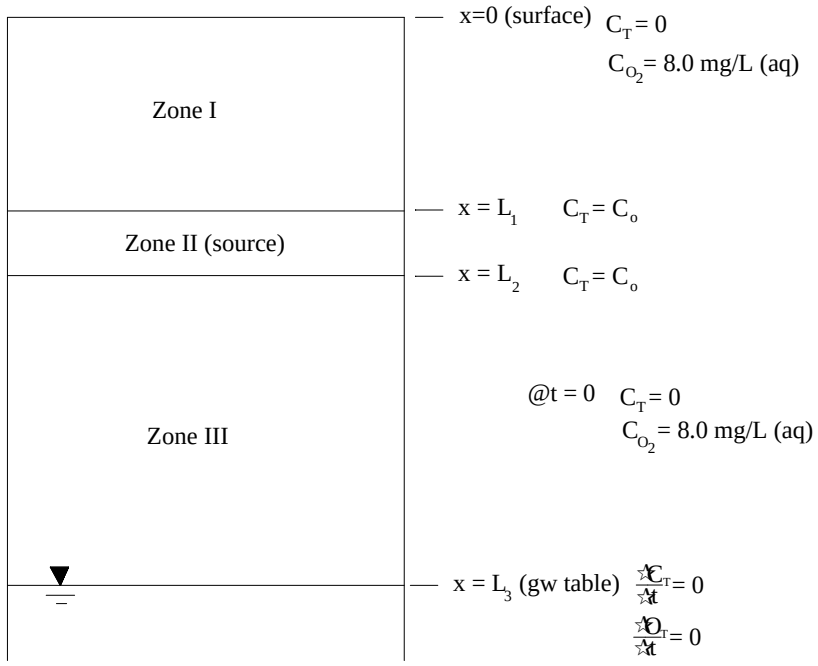

Figure 5-1. A common physical scenario.

For oxygen there is only one zone and therefore we need only one governing equation, one IC, and one set of BC's.

$$@\, t = 0 \qquad C_{O_2} = 8 \ mg/L \ (aq) \tag{5.1}$$

$$@\, x = 0 \ \ (\text{surface}) \qquad C_{O_2} = 8 \ mg/L \ (aq) \tag{5.2}$$

$$@\, x = L_3 \ \ (\text{gw table}) \qquad \frac{\partial O_T}{\partial t} = 0 \tag{5.3}$$

For hydrocarbon we need one equation, one IC and one set of BC's for each unsaturated zone (Zone I & Zone III). If we use the typical scenario as shown in Figure 5-1, we get the following conditions for Zone I (where C_o is the hydrocarbon equilibrium concentration in the aqueous phase):

$$@\, t = 0 \qquad C_T = 0 \tag{5.4}$$

$$@\, x = 0 \ \ (\text{surface}) \qquad C_T = 0 \tag{5.5}$$

$$@\, x = L_1 \qquad C = C_O \tag{5.6}$$

For Zone III we get:

$$@\,t = 0 \qquad C_T = 0 \tag{5.7}$$

$$@\,x = L_2 \qquad C = C_O \tag{5.8}$$

$$@\,x = L_3 \ \text{(gw table)} \qquad \frac{\partial C_T}{\partial t} = 0 \tag{5.9}$$

For the source zone (Zone II), we need only the IC of separate phase liquid with a equilibrium concentration specified (C_o).

We will use benzene as our hydrocarbon compound because of its health risk and it's common mobility in the subsurface environment. This will be used to find the stoichiometric constant (F) for the gasoline mixture in the following stoichiometric equation where we assume complete mineralization to carbon dioxide and water:

$$C_6H_6 + 7.5\,O_2 \rightarrow 3\,H_2O + 6\,CO_2 \tag{5.10}$$

$$F = \frac{\text{mass oxygen}}{\text{mass hydrocarbon}} = \frac{7.5 \cdot 32.00}{78.1134} = 3.07 \tag{5.11}$$

where 7.5 is the O_2 coefficient necessary to balance the above stoichiometric equation, 32.00 is the molecular weight of oxygen, and 78.1134 is the molecular weight of the benzene.

In this separate phase example we will use a typical water content profile described by the following graph.

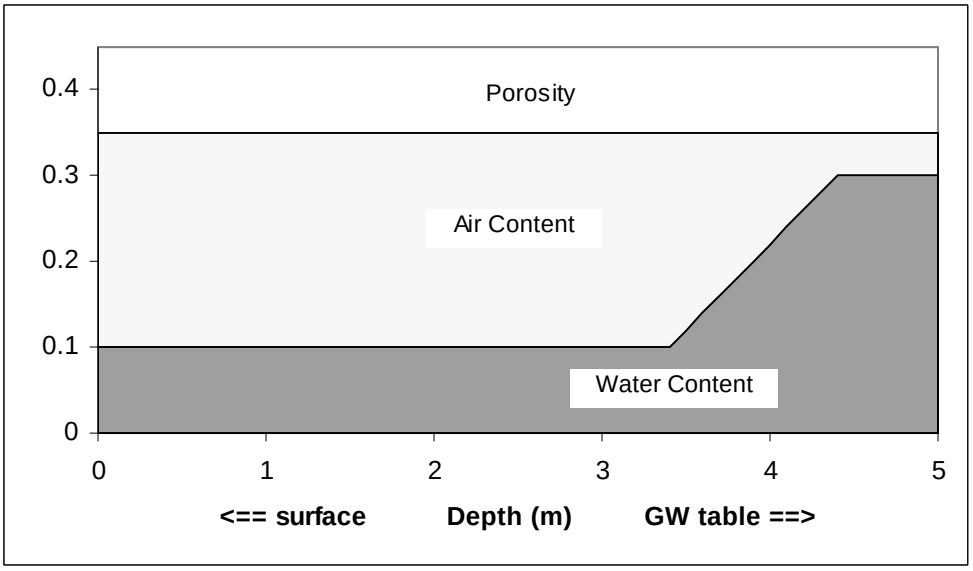

Figure 5-2. Common water content profile.

The parameters used in this simulation are given below:

Table 5-1. Numerical Parameters.

Name	Value (common units)	(SI Units)
Δt	2 days	2 days
Δx	0.05 m	0.05 m
Length of source	0.6 m	0.6 m
Length of Zone I (above)	2.0 m	2.0 m
Length of Zone III (below)	2.4 m	2.4 m

[a] based on a common mole fraction of benzene in gasoline
[b] From Henry's Law: equation 2.15
[c] we assume atmospheric conditions of 21% oxygen (units converted using the Ideal Gas Law)

Table 5-2. Parameters of Monod Kinetics.

Name	Value (common units)	(SI Units)
microbial cell concentration (M_t)[a]	0.23 mg/L	0.00023 kg/m^3
maximum utilization rate (k_m)[b]	6.8 day^{-1}	6.8 day^{-1}
stoichiometric constant (F)[c]	3.07	3.07
half saturation constant (benzene) (K_s)[a]	0.65 mg/L	0.00065 kg/m^3
half saturation constant (oxygen) (K_{s,O_2})[a]	0.1 mg/L	0.0001 kg/m^3

[a] From MacQuarrie et. al. (1990)
[b] From Tabak (1991)
[c] From equation 5.10

Table 5-3. Physical Parameters.

Name	Value (common units)	(SI Units)
vapor diffusion of benzene (D_a)[a]	0.829 m^2/d	0.829 m^2/d
aqueous diffusion of benzene (D_w)[a]	0.0001161 m^2/d	0.0001161 m^2/d
vapor diffusion of oxygen (D_{a,O_2})[a]	1.6857 m^2/d	1.6857 m^2/d
aqueous diffusion of oxygen (D_{w,O_2})[a]	0.0001814 m^2/d	0.0001814 m^2/d
Benzene equilibrium conc. in water phase[a]	5.0 mg/L	0.005 kg/m^3
initial oxygen conc. in water[b]	8.0 mg/L	0.008 kg/m^3
initial oxygen conc. in air[c]	287 mg/L	0.287 kg/m^3
benzene cut off concentration	0.3 mg/L	0.0003 kg/m^3
oxygen cut off concentration	1.0 mg/L	0.001 kg/m^3
Henry's Law constant (benzene)[a]	0.224	0.224
Henry's Law constant (oxygen)[b]	35.875	35.875
K_d (benzene)[c]	8.29 L/kg	0.00829 m^3/kg
bulk density (ρ_b)	1.6 kg/L	1600 kg/m^3
benzene oil content (θ_o)	0.10	0.10
specific density of benzene (ρ_o)	800,000 mg/L	800 kg/m^3

[a] From Schwarzenbach et. al. (1993)
[b] From Henry's Law: equation 2.15
[c] From equations 3.8, 3.9, and 3.10 assuming an organic fraction of 1% and the properties of benzene

Results

Figure 5-3 shows the coupled benzene and oxygen concentrations for the scenario where a separate phase liquid exists in the middle of the vadose zone. The plot shows the oxygen and benzene concentrations in the aqueous phase for 7 time series. It can be seen that the separate phase source lasts for several years. Under natural conditions capillary forces would pull the source downward toward the water table as the data from the previous validations show. This model does not include separate phase transport, but is only concerned with the diffusion and biodegradation of the vapors that are released from the separate phase.

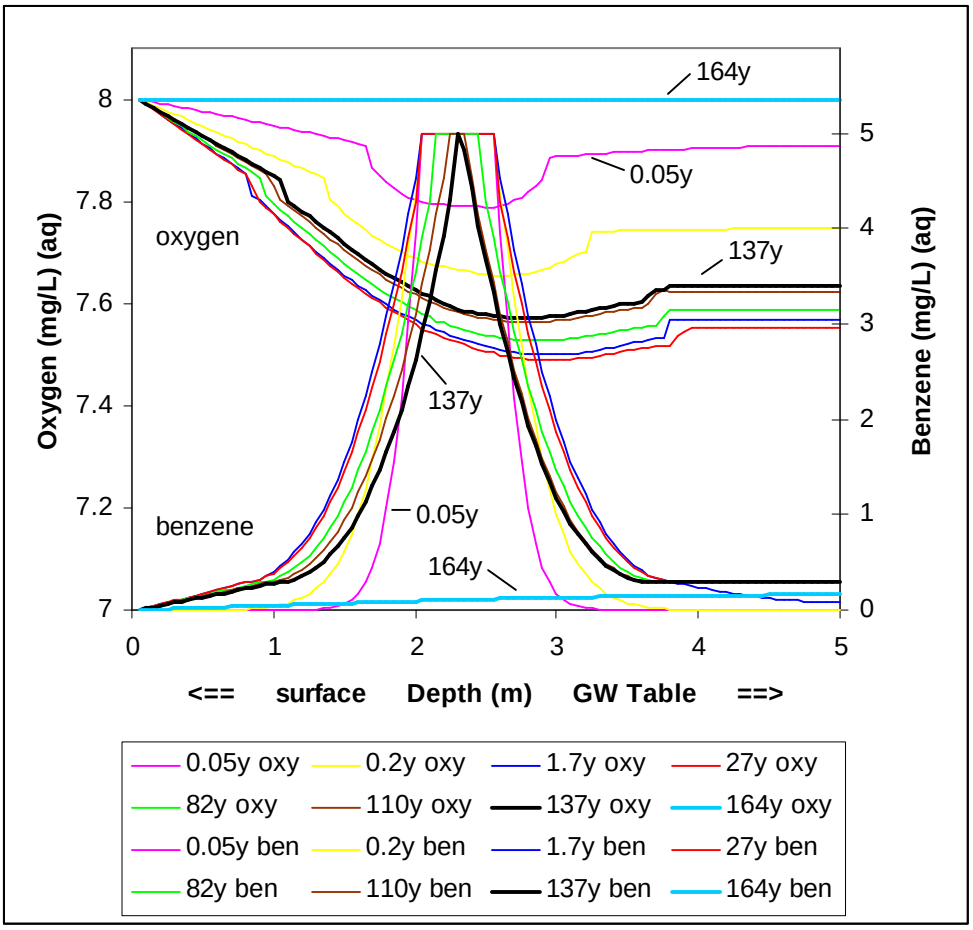

Figure 5-3. Concentration results.

We can see from the right side of Figure 5-3 (i.e. the water table) how the Type II boundary conditions of no flow effect the oxygen concentration as they reach the water table. The constant benzene concentration near the center of the vadose zone (~ 2.5 meters) at 5 mg/L shows that the separate phase still exists.

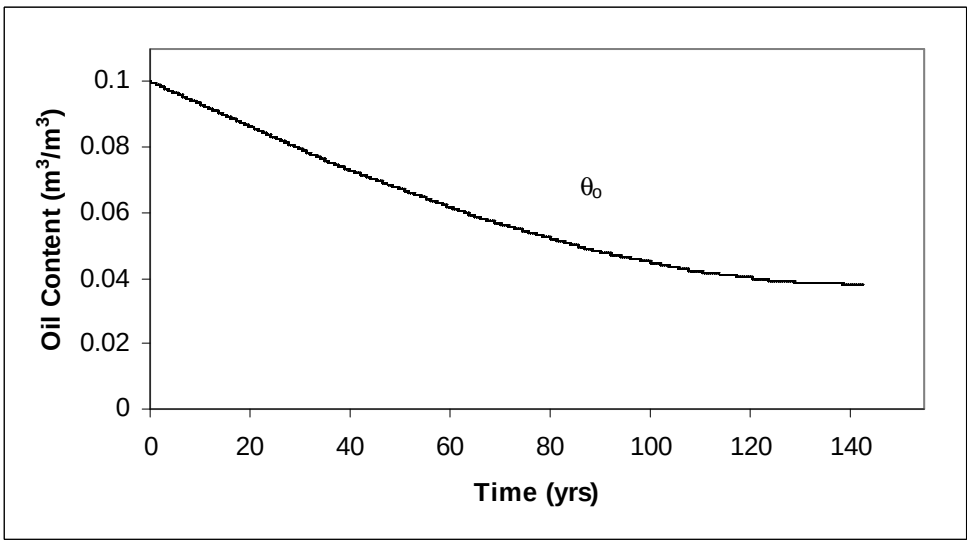

Figure 5-4. Change in oil content due to biodegradation over time.

Figure 5-4 shows that the benzene oil content decreases over time. Within the source zone (Zone II of Figure 5-1), the oxygen continues to diffuse and is available for biodegradation to proceed. There appears to be a decreasing rate in the oil content. This is explained by the fact that the rate is dependent on the oxygen concentration which also decreases over time.

Figure 5-5 shows that the thickness or length of the source shrinks over time. From Figure 2-2 we see how this is accomplished.

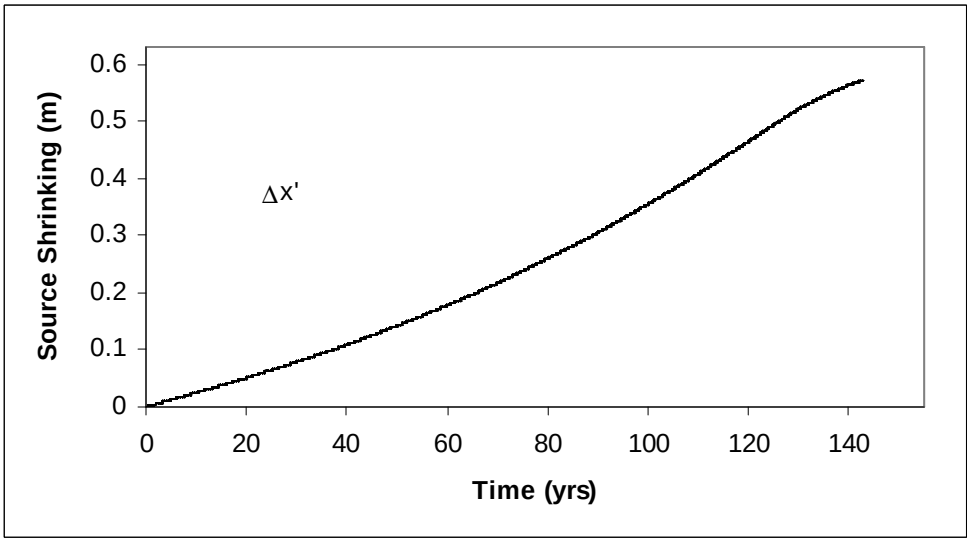

Figure 5-5. Change in source length over time due to diffusive flux.

The oil content used is based on benzene only. If we were to include multiple compounds in our model, we would have to have separate Monod kinetics for each compound and bookkeep their mole fraction in the separate phase liquid.

If there was no biodegradation, then in Zone I the benzene concentration would be linear from 5 mg/L at the source to 0 mg/L at the surface (BC). This shows that biodegradation is a very significant component in the clean up process and is very important in decision making management based on risk to human health. Under this condition, we would have a very significant in-flux of vapors into the building or surface. In Zone III similar conclusions can be made about the significance of biodegradation. If no biodegradation were to occur in this zone then the pore space would fill completely with contaminated vapors, since we have set a no flow boundary condition at the water table for the hydrocarbon. Though through partitioning, we would see hydrocarbon compounds entering the groundwater as a dissolved phase.

6.0 Conclusion

When soils are impacted by spills or leaks, there is an increased potential for contamination via vapor migration to enclosed spaces. This pathway plays an important role in decision-making management. The focus on vapor transport pathways has been brought about mainly by the move toward a more structured risk-based corrective action (RBCA).

The risk associated with vapor intrusion and the potential remediation by natural attenuation of vapors in the vadose zone is currently a hot topic (Johnson 1998). Many feel that the current models are too conservative and lead to unnecessary low cleanup levels. Since these models generally do not take into account natural biodegradation, extreme cleanup requirements are set. The model we have developed takes into account biodegradation and simulates the fate and transport of hydrocarbon and oxygen vapors.

In order to assess and predict the fate and migration of hydrocarbon vapors in the vadose zone, we have developed a simple model. This model simulates the diffusion of hydrocarbon and oxygen in the vapor and aqueous phases of the unsaturated zone as well as the degradation due to biological factors. The vapor transport of oxygen and hydrocarbon is thus a coupled balance of diffusion and biological degradation or biodegradation. To simplify the model for our purposes, we have developed a single component model and have neglected advection and the movement of the source zone.

To show the significance of biodegradation as a cleanup method, we have taken the data measured at a US Coast Guard Air Station in Traverse City, Michigan, where high levels of hydrocarbon vapors throughout the vadose zone were detected. A release of more than 100,000 kg of aviation fuel entered the subsurface 30 years ago and in 1991 existed as a separate phase liquid in the capillary fringe. The dimensions of the plume were 80 meters wide and 250 meters long and confined to a 0.3-meter thickness. The water table was measured to be 5.44 meters below the soil surface.

The second site where we demonstrated the significance of biodegradation consists of a former gasoline station located at the Alameda Naval Air Station in California. Almost 20 years ago their underground storage tanks leaked and high concentrations of hydrocarbon vapors were later detected in the soil, and trace amounts found in the building itself, the highest of which was Isopentane (0.026 μg/L). The depth to the water table here was only 1.92 meters.

We then created an example where a separate phase liquid exists in the middle of the vadose zone where we have unsaturated soil above and beneath the source zone. The purpose of this example was to quantify the contamination potential to the surface and to the groundwater. It was also desirous to determine the source longevity by modeling the shrinking of the source.

By applying the model to these three examples, we see that biodegradation is a significant component in the cleanup process. Had we neglected biodegradation, the simulated hydrocarbon concentrations would be linear from the source up to the surface. The flux entering the building or leaving the soil surface is then calculated using the difference in the last two nodal concentration values. For enclosed spaces such as basements, a ventilation procedure can be implemented to determine the concentration of vapors that pose hazardous health threats. By including biodegradation, the concentration at the second to last node is significantly reduced in all three examples and hence the degree of over-conservatism is lessened. This procedure is still an over-estimation since we assume a zero concentration boundary condition, but is still a much more accurate estimation than without. Since low cleanup level remediation technologies are very expensive, it appears clear that natural attenuation should be considered in determining these low-level concentration requirements.

In order to get an accurate simulation of coupled fate and transport of oxygen and hydrocarbon, more data are required regarding the oxygen availability and specifically the boundary condition at the surface. Since oxygen can be depleted by consumption from vegetation in the root zone and consumption due to other microbial activity not related to petroleum hydrocarbons, it is necessary to quantify this and provide a realistic oxygen concentration at the boundary.

Based upon our conclusions, biodegradation and risk-based decision making deserves further research and attention. One such approach is to develop a multi-component model where we could analyze each of the several components and determine a proper source longevity and potential vapor concentration risk to enclosed spaces such as basements. Advection could be included as well. Advection may be caused by density gradients that arise due to differences in partitioning coefficients of the individual hydrocarbon species. The density driven advection could be compared to GC/MS analysis of the vapors collected. Individual gasoline components would be expected to separate chromatographically with increasing elevation, leading to species dependent profiles through the vadose zone, with a potential for a structured microbiological profile in response. Further research along these lines may prove useful. Another approach is to look at carbon dioxide concentrations. For the Michigan site, Kampbell et al. (1990) measured carbon dioxide concentrations at Traverse City, which could be considered in the stoichiometry assumption.

In conclusion, one of the main reasons for including the aqueous phase diffusion is the fact that near the water table the vapor pore space is small and the water content is near the porosity value. Under these conditions the aqueous diffusion process becomes more significant than usual, while the vapor diffusion process becomes less dominant. When the separate phase source is emerged in the capillary fringe, then the pore space above is completely saturated and the vapor diffusion becomes non-existent and the only diffusion mechanism is the aqueous diffusion.

The fluctuating of the water table plays an important role in vapor pathway exposure. The overall conclusion is that an accurate soil moisture profile is almost essential in fitting the data to the model. The reason for this is due to equation 2.4, especially near the water table where the air content is very small. The sensitivity of the diffusion coefficient near the water table cannot be over emphasized. With the increased use of risk-based decision making and RBCA, it is becoming clear that in situ measurements of diffusion coefficients are becoming increasingly necessary (Johnson et. al. 1998). Perhaps more detailed soil moisture data (temporal and spatial) would lead to a better understanding of contaminated vapor fate and transport in the subsurface.

7.0 References

Allen-King, R.M., Groenevelt, H., Warren, C.J., and Mackay, D.M., Non-linear chlorinated-solvent sorption in four aquitards, *J. Contam. Hydrol.* vol. 22, no. 3-4, pp. 203-221 1996.

Borden, R.C. and Bedient, P.B., Transport of Dissolved Hydrocarbons Influenced by Oxygen-Limited Biodegradation 1. Theoretical Development, *Water Resour. Res*., Vol. 22, No. 13, pp. 1973-1982, December 1985.

Falta, R.W., Javandel, I., Pruess, K., and Witherspoon, P.A., Density-Driven Flow of Gas in the Unsaturated Zone Due to the Evaporation of Volatile Organic Compounds, *Water Resour. Res*., Vol. 25, No. 10, pp. 2159-2169, October 1989.

Fischer, M.L., Bentley, A.J., Dunkin K.A., Hodgson, A.T., Nazaroff, W.W., Sextro R.G., and Daisey, J.M., Factors Affecting Indoor Air Concentrations of Volatile Organic Compounds at a Site of Subsurface Gasoline Contamination, *Environ. Sci. Technol*., Vol. 30, No. 10, pp. 2948-2957, 1996.

Hinchee, R.E., and Reisinger, H.J., Multi-Phase Transport of Petroleum Hydrocarbons in the Subsurface Environment: Theory and Practical Application, in *Proceedings Petroleum Hydrocarbons and Organic Chemicals in Groundwater*, pp. 58-76, National Well Water Association/American Petroleum Institute, Dublin, Ohio, 1985.

Howard, P.H., and Meylan, W.M., Handbook of Physical Properties of Organic Chemicals, Lewis Publishers, New York, 1997.

Johnson, P.C., Kemblowski, M.W., and Johnson, R.L., Assessing the Significance of Subsurface Contaminant Vapor Migration to Enclosed Spaces: Site-Specific Alternative to Generic Estimates, API 4674, December 1998.

Johnson, P.C., Bruce, C., Johnson, R.L., and Kemblowski, M.W., In Situ Measurement of Effective Vapor-Phase Porous Media Diffusion Coefficients, *Environ. Sci. Technol*., 32, 3405-3409, 1998.

Jury, W.A. *Soil Physics*, p. 328 J.Wiley, New York, 1991

Kemblowski, M.W., and Ma, Y., Modeling aerobic biodegradation of dissolved hydrocarbons in heterogeneous geologic formations, Report to American Petroleum Institute, HydroGaia, Inc., Nibley, Utah, June 1994

Li, C., and Voudrias, E.A., Migration and sorption of jet fuel aliphatic vapors in unsaturated soil. *Water Res.* vol. 28, no. 12, pp. 2447-2456, 1994.

Lyman, Warren J. *Handbook of chemical property estimation methods*, Washington, DC: American Chemical Society, 1990.

MacQuarrie, K.T.B., Sudicky, E.A., and Frind, E.O., Simulation of Biodegradable Organic Contaminants in Groundwater: 1. Numerical Formulation of Principal Directions, *Water Resour. Res*., Vol. 26, No. 2, pp. 207-222, February 1990.

McClure, P.D. and Sleep, B.E., Simulation of bioventing for soil and ground-water remediation, *J. Environ. Eng.* Vol. 122, No. 11, pp. 1003-1012, 1996.

Millington, R.J., and Quirk, J.P., Permeability of porous solids, *Trans. Faraday Soc*., pp. 1200-1207, 1961.

Ostendorf, D.W. and Kampbell, D.H., Bioremediated soil venting of light hydrocarbons, *Hazard Waste Hazard Mater.*, Vol. 7, pp. 319-334, 1990.

Ostendorf, D.W. and Kampbell, D.H., Biodegradation of Hydrocarbon Vapors in the Unsaturated Zone, *Water Resour. Res.*, Vol. 27, No. 4, pp. 453-462, April 1991.

Pfannkuch, H.O., Determination of the contaminant source strength from mass exchange processes at the petroleum groundwater interface in shallow aquifer systems, in *Proceedings Petroleum Hydrocarbons and Organic Chemicals in Groundwater*, pp. 111-129, National Well Water Association/American Petroleum Institute, Dublin, Ohio, 1984.

Refsgaard, J.C., Christensen, T.H., and Ammentorp, H.C., A model for oxygen transport and consumption in the unsaturated zone, *Journal of Hydrology*, vol. 129, pp. 349-369, 1991

Rich, L.G. *Environmental Systems Engineering*, p. 447 McGraw Hill, New York, 1973.

Schwarzenbach, R.P., Gschwend, P.M., Imboden, D.M., *Environmental Organic Chemistry*, pp194-238, J. Wiley, New York, 1993.

Semprini, L., and McCarty, P.L., Comparison Between Model Simulations and Field Results for In-Situ Biorestoration of Chlorinated Aliphatics: Part 1. Biostimulation of Methanotrophic Bacteria, *Ground Water*, 23 (3), 1991.

Tabak, H. H., *Development of predictive structure biodegradation relationship models*, Washington, D.C. : U.S. Environmental Protection Agency, 1991.

Yakowitz, S., and Szidarovszky, F., *An introduction to Numerical Computations*, pp. 95-96, Macmillan Collier, New York, 1989.